Bone Reports 29 (2026) 101924

Contents lists available at ScienceDirect

Bone Reports

journal homepage: www.elsevier.com/locate/bonr

Deep phenotyping of an ATDC5 in-vitro cartilage model system

Anna Klawonn [a,b,c,d], Stefan Tholen [e,f], Ilona Skatulla [a], Chiara M. Schröder [b,c,g], Sebastian J. Arnold [b,g], Oliver Schilling [e,f], Miriam Schmidts [a,b,c,*]

[a] Center for Pediatrics and Adolescent Medicine, Medical Center - University of Freiburg, Freiburg, Germany
[b] CIBSS - Centre for Integrative Biological Signalling Studies, University of Freiburg, Freiburg, Germany
[c] Spemann Graduate School of Biology and Medicine (SGBM), Freiburg, Germany
[d] Faculty of Biology, University of Freiburg, Freiburg, Germany
[e] Institute for Surgical Pathology, Medical Center – University of Freiburg / Medical Faculty – University of Freiburg, Germany
[f] Proteomics Platform – Core Facility (ProtCF), Medical Center – University of Freiburg / Medical Faculty – University of Freiburg, Germany
[g] Institute of Experimental and Clinical Pharmacology and Toxicology, Faculty of Medicine, University of Freiburg, Germany

ARTICLE INFO

Keywords:
Chondrogenesis
Cartilage
ATDC5
Extracellular matrix
Proteomics

ABSTRACT

Cartilage is characterized by a highly specialized extracellular matrix (ECM) secreted by chondrocytes and limited self-regenerative capacity. In vivo investigations of chondrogenesis are limited by difficult and traumatic access, especially in humans. While it is known for decades that disturbances of chondrocyte differentiation and changed cartilage ECM composition cause severe skeletal phenotypes in vertebrates, a detailed molecular understanding of chondrogenesis and cartilage ECM formation is still missing, especially in the context of human genetic skeletal diseases.

ATDC5 cells, derived from AT805 mouse teratocarcinoma cells, have been used in the past to model chondrogenic differentiation, however, most studies have investigated few major cellular differentiation markers only so that the composition of the secreted ECM as well as effects on the ATDC5 transcriptome upon differentiation are still unclear. Here, we performed time-resolved transcriptomic and ECM proteomic analyses of differentiating ATDC5 cells. Both datasets confirmed the formation of a cartilage-like matrix with increasing expression of key chondrocyte genes over the course of differentiation. ECM proteomics further revealed a number of ECM components not previously reported in ATDC5 cells or the secreted ECM, encompassing collagens, proteoglycans, glycoproteins and other secreted factors. Overall, our findings provide a more detailed molecular characterization of ATDC5 chondrogenesis and highlight the potential of this model system for ECM-focused studies.

1. Introduction

Cartilage is a unique tissue characterized by a low cellular density and an abundant, highly specialized extracellular matrix (ECM) secreted by chondrocytes (Bačenková et al., 2023). This matrix is predominantly composed of collagens and proteoglycans which together determine the characteristic mechanical properties of cartilage (Han et al., 2011; Hsueh et al., 2016). Collagen fibrils form a stable and tensile network (Svensson et al., 2010), whereas highly water-binding proteoglycans confer elasticity and resistance to compressive forces (Farach-Carson et al., 2024). In addition, non-collagenous proteins contribute to the interconnection of supramolecular structures, fibril assembly, matrix integrity, and cell-matrix interactions (Gao et al., 2014; Grässel and Aszódi, 2016). Understanding the process of chondrogenesis, ECM composition and homeostasis, and the interactions between chondrocytes and their surrounding matrix is of considerable interest. This knowledge is not only critical for elucidating defects in endochondral bone formation (Unger et al., 2023), but is also of importance for advancing human cartilage tissue engineering, as the treatment of cartilage injuries and degenerative diseases, such as osteoarthritis, remain a challenge in modern regenerative medicine (Welsh and Sikder, 2025).

Chondrogenesis is a multistep process that begins with the condensation of mesenchymal progenitor cells, followed by their differentiation into mature chondrocytes. During endochondral bone formation, these cells subsequently progress through a proliferating, then

* Corresponding author at: Department of Pediatrics, Adolescent Medicine and Neonatology Medical Center – University of Freiburg Faculty of Medicine, Breisacher Straße 86, 79106, Freiburg, Germany.
E-mail address: miriam.schmidts@uniklinik-freiburg.de (M. Schmidts).

https://doi.org/10.1016/j.bonr.2026.101924
Received 16 April 2026; Received in revised form 21 May 2026; Accepted 26 May 2026
Available online 28 May 2026

prehypertrophic stage and further differentiate into hypertrophic chondrocytes. Hypertrophic chondrocytes exit the cell cycle and contribute to the mineralization and remodeling of the late ECM, which is subsequently replaced by bone (Goldring et al., 2006). Notably, terminal hypertrophic differentiation does not occur in healthy articular cartilage (Chawla et al., 2022). To investigate chondrogenesis, a variety of experimental models have been established. In addition to established cell lines such as ATDC5 (Atsumi et al., 1990) or C3H10T1/2 (Shea et al., 2003), induced pluripotent stem cells (iPSCs) (Wu et al., 2021) and mesenchymal stem cells (MSCs) (Huynh et al., 2019; De la Fuente et al., 2012; Schwarzl et al., 2023) have been used to study transcriptional dynamics and ECM development during chondrogenesis. Stem-cell based approaches however are limited by donor variability, limited reproducibility, restricted cell availability and replicative senescence (Casorati et al., 2025; Riss et al., 2021; Česnik and Švajger, 2024). Hence, simpler models such as ATDC5 cells offer an advantage of higher robustness, reproducibility and scalability as well as effective gene editing possibilities for comparative studies of genetic variations.

The ATDC5 model system has been widely used to study chondrogenesis since its first description in 1990 by Atsumi et al. (1990) who also established the cell line and successfully induced differentiation by supplementing the growth medium with insulin, transferrin and sodium selenite, a protocol which still remains a standard today. Subsequently, additional supplements such as ascorbic acid or β-glycerophosphate have been introduced to accelerate chondrogenic differentiation (Altaf et al., 2006; Okita et al., 2023; Temu et al., 2010) or enhance matrix mineralization (Newton et al., 2012; Huitema et al., 2006).

Surprisingly, despite more than 1000 PubMed entries related to ATDC5 cells as of January 2026, a comprehensive and unbiased characterization of ATDC5 gene expression patterns during differentiation as well as composition of the secreted ECM are still lacking: most studies using ATDC5 cells have followed the expression of only few chosen chondrocyte marker genes (Hissnauer et al., 2010) such as *Sox9, Col2a1* and *Col10a1*. Moreover, only a single study (Wilhelm et al., 2020) has performed an extensive proteomic characterization of ATDC5 ECM. A systematic characterization of the temporal transcriptional and extracellular matrix landscape of ATDC5 differentiation therefore provides an essential framework for future mechanistic studies.

Here, we combined time-resolved transcriptomic analyses with ECM-focused proteomics to provide an integrated characterization of transcriptional dynamics and matrix composition during ATDC5 chondrogenesis.

2. Materials and methods

2.1. Cell culture

ATDC5 cells were obtained from ECACC. Cells were cultured in medium composed of Dulbecco's modified eagle medium (DMEM, 32430100, Gibco™, Thermo Fisher Scientific, Waltham, MA, USA) and Ham's F-12 (11765054, Gibco™, Thermo Fisher Scientific, Waltham, MA, USA) in a ratio of 1:1, supplemented with 10% fetal calf serum (FCS, F7524 Sigma, Taufkirchen, Germany), 1% Sodium Pyruvate (S8636, Sigma, Taufkirchen, Germany), 100 U/ml penicillin and 100 μg/ml streptomycin (P-0781, Sigma, Taufkirchen, Germany) at 37 °C and 5% CO_2. The cells were passed every 3–4 days.

For differentiation experiments, ATDC5 cells were plated at 3×10^5 or 0.75×10^5 cells/well into 6 or 12-well plates (83.3920/ 83.392, Sarstedt, Nümbrecht, Germany) and differentiation was initiated upon confluency under identical standardized conditions in all biological replicates. For induction, the growth mediums FCS concentration was reduced to 5% and the medium was supplemented with 10 μg/ml insulin (I9278, Sigma, Taufkirchen, Germany), 30 nM sodium selenite (S5261, Sigma, Taufkirchen, Germany), 50 μg/ml ascorbic acid (A4403, Sigma, Taufkirchen, Germany) and 10 μg/ml transferrin (90190, Sigma, Taufkirchen, Germany). The medium was changed every other day. The selected time points (day 0, 4, 7, 14, and 21) were used as the primary sampling scheme for transcriptomic and proteomic analyses and were chosen to cover early, intermediate, and late phases of ATDC5 chondrogenic differentiation, as described previously for this model system (Altaf et al., 2006; Yuan et al., 2022).

2.2. Proteoglycan and collagen staining

Cells were washed twice with PBS (D8537, Sigma, Taufkirchen, Germany) and fixed with ice-cold methanol. At day 0, 4, 7, 14 and 21, cells were stained for proteoglycans and collagens using 0.1% Alcian Blue (A5268, Sigma, Taufkirchen, Germany) in 0.1 M HCl and Sirius Red solution (13422, Morphisto, Offenbach am Main, Germany) for 2 h at room temperature. Following incubation, excess dye was removed. Alcian Blue-stained cells were rinsed with PBS, while Sirius Red-stained cells were washed with 0.01 M HCl to remove unbound dye. Images of the stained cultures were captured using a Leica microscope or phone camera.

2.3. Immunohistochemistry

Cells were seeded on gelatin-coated cover slips and maintained until they reached confluency, then differentiation was induced. At day 4, cells were washed three times with PBS, fixed with 4% PFA solution. After blocking with 5% BSA in PBS solution the fixed cells were stained with rabbit anti-fibronectin antibody (1:500, ab2413, abcam, Cambridge, United Kingdom) for 2 h at room temperature. Cells were then washed three times with PBS and incubated with Alexa 488 Goat Anti Rabbit (1:500, A11008, Thermo Fisher Scientific, Waltham, MA, USA). Cells were finally washed three times with PBS and mounted in Vectashield with DAPI (VEC-H-1200, Biozol, Hamburg, Germany). Images were taken with a Leica THUNDER Imager (Leica, Wetzlar, Germany) with a 63× objective.

2.4. Proliferation assay

Cell proliferation was assessed at day 0, 4 and 7 using the Click-iT™ Plus EdU Alexa Fluor™ 555 Imaging Kit (C10638, Thermo Fisher Scientific, Waltham, MA, USA) following the manufacturer's instructions. Briefly, cells were seeded on coverslips and incubated with 10 μM EdU (5-ethynyl-2′-deoxyuridine) for 2 h at the indicated time points. After incubation, cells were fixed with PFA 5% in PBS, permeabilized with Triton 0.5% in PBS, and subjected to the Click-iT™ Plus reaction cocktail for EdU detection. Cover slips were mounted in Vectashield with DAPI. Fluorescent images were acquired at different spots on the cover slip. EdU incorporation was evaluated by analyzing 3 images, but at least 100 nuclei, per time point.

2.5. RNA sequencing

RNA was extracted from cells grown in 6-well plates at day 0, 4, 7 14 and 21 of differentiation, using RNeasy Fibrous Tissue Mini Kit (74704, Qiagen, Hilden, Germany) according to the protocol provided by the manufacturer. RNA concentration was measured with Nano Drop ND-1000 (Thermo Fisher Scientific, Waltham, MA, USA). RNA quality was assured by measurement of RNA integrity value using High Sensitivity RNA Screen Tape Analysis (Tape Station 4150, Part number 5067 5579, Agilent technologies, Santa Clara, CA, USA). RNA sequencing of four replicates per time point was performed at Novogene, Hongkong. For each sample 5 GB raw data were available. All RNA sequencing data generated in this study have been deposited in the Gene Expression Omnibus under accession number GSE324360.

2.6. Transcriptomics bioinformatics

RNA-Seq data analysis was performed using the Galaxy web platform

(usegalaxy.eu, Galaxy). Raw sequencing reads were first quality-checked using FastQC (version 0.74 + galaxy1), and adapter trimming was carried out with Trim Galore! (version 0.6.7 + galaxy0). One sample at this time point could not be processed in Galaxy for unknown reasons. As three additional biological replicates were available, this sample was excluded from downstream analysis. Cleaned reads were then mapped to the mouse reference genome (GRCm39) using RNA STAR (version 2.7.11a + galaxy1) as paired end data and "length of the genomic sequence around annotated junctions" set to 149. Read counts per gene were quantified using featureCounts (version 2.0.6 + galaxy0) with GENCODE comprehensive gene annotation for mouse (GRCm39, release M35; Ensembl 112). The resulting count matrix was used as input for differential gene expression analysis in DESeq2 (version 2.11.40.8 + galaxy0) within Galaxy. Normalized count files were used for the generation of dot plots encoding gene-wise z-scores by color and scaled values by point size, using the pheatmap package in R. GO term enrichment analysis was conducted using the Functional Annotation tool in DAVID (Sherman et al., 2022) to identify significantly enriched biological processes. GO enrichment analyses were conducted using the complete gene sets, unless when a high proportion of not annotated genes hampered GO analyses in which case not annotated genes were excluded from GO analysis; such cases are indicated in the figure legends. Graphs and Volcano plots were created using Prism10 GraphPad Software (v10.5.0, GraphPad Software, Boston, MA, USA).

For creating the k-means clustered heatmap the results were filtered for adjusted $p < 0.05$ and $\log_2$(fold change (FC)) ± 2 as indicated in the figure legends. Before fitting and statistical analysis, counts were normalized by library size (DESeq2::estimateSizeFactors) and gene-wise dispersion (DESeq2::estimateDispersions) to normalize the gene counts by gene-wise geometric mean over samples. For plotting the heat maps, gene-wise scaling was performed on the normalized counts to cluster the counts for the expression tendency between the samples (stats::kmeans function). In addition, the counts were centred by setting the gene-wise mean to zero, which explains why some count values are negative (below gene-wise mean). Visualization of the clustered data was performed using the pheatmap::pheatmap function (pheatmap v.1.0.10) with deactivated function-intrinsic clustering.

2.7. ECM proteomics

ECM proteomic samples were drawn at day 0, 4, 7, 14 and 21 of differentiation and subjected to label-free quantitative LC-MS/MS analysis using an Evosep One system (Evosep Biosystems, Odense, Denmark) coupled to a timsTOF fleX mass spectrometer (Bruker, Billerica, MA, USA). ATDC5 cells were cultured in differentiation medium until harvest. ECM proteins were derived from the cell-deposited matrix remaining after decellularization. Cells were removed by incubating the sample with decellularization buffer (20 mM NH_4OH, 0.5% Triton X-100), followed by extensive PBS washing and 30 min DNAseI (15 U/ml, 79254, Qiagen, Hilden, Germany) treatment. Lysis of remaining ECM and preparation for mass spectrometry analysis was performed as described previously (Busch et al., 2024). Peptides were analyzed with the Evosep One system (Evosep Biosystems, Odense, Denmark) coupled to a timsTOF fleX mass spectrometer (Bruker, Billerica, MA, USA). 500 ng of peptides were loaded onto Evotips C18 trap columns (Evosep Biosystems, Odense, Denmark) according to the manufacturer's protocol. Peptides were separated on an EV1137 performance column (15 cm × 150 µm, 1.5 µm, Evosep, Odense, Denmark) using the standard implemented 30 SPD method with a gradient length of 44 min (buffer A: 0.1% *v*/v formic acid, dissolved in H_2O; buffer B: 0.1% v/v formic acid, dissolved in acetonitrile). Over the time of the gradient, the concentration of acetonitrile gradually increased from 0 to 90% at a flow rate of 500 nl/min.

The timsTOF fleX mass spectrometer (Bruker, Billerica, MA, USA) was operated in the DIA-PASEF mode. DIA MS/MS spectra were collected in the range in an *m/z* range from 100 to 1700. Ion mobility resolution was set to 0.60–1.60 V·s/cm over a ramp time of 100 ms and an accumulation time of 100 ms. The cycle time was set at 1.8 s. The collision energy was programmed as a function of ion mobility, following a straight line from 20 eV for 1/K0 of 0.6 to 59 eV for 1/K0 of 1.6. The TIMS elution voltage was linearly calibrated to obtain 1/K0 ratios using three ions from the ESI-L TuningMix (Agilent) (*m/z* 622, 922, 1222).

Raw data were analyzed with DIA-NN software (v.2.0) (Demichev et al., 2020). A spectral library was predicted using a FASTA file containing the murine protein sequences as of June 23rd, 2025 (mouse-EBI-reference database, https://www.ebi.ac.uk/). The false discovery rate (FDR) was set to 1%. The search was performed allowing one missed cleavage and cysteine carbamidomethylation enabled as a fixed modification. Match between runs was enabled. Quantification was performed using the label-free quantification algorithm MaxLFQ, which calculates the protein quantities as ratios from all peptide intensities.

The data was further processed and analyzed for the statistical analysis using R (v4.3.0) within R studio. All samples were processed in a single experimental run; thus, no batch correction was required. Protein intensities were log2-transformed and median normalized. Differential expression analysis was performed using limma (Ritchie et al., 2015). *P*-values were corrected by multiple testing using the Benjamini–Hochberg method, as applied by limma. Mass spectrometry raw data have been deposited at the ProteomeXchange Consortium (http://proteomecentral.proteomexchange.org) under the accession number PXD074419. Furthermore all mass spectrometry proteomics datasets used and/or analysed during this study are available online at the MassIVE repository (http://massive.ucsd.edu/; dataset identifier: **MSV000100830**.). This study did not generate new code for analysis.

Dot plots encoding gene-wise z-scores by color and scaled values by point size were generated using the pheatmap package in R. For creation of Venn Diagrams interactivenn web tool was used (Heberle et al., 2015).

2.8. Statistical analysis

Data are presented as mean ± SD. Statistical analyses were performed using appropriate tests as indicated in the figure legends. For proliferation analysis two-way ANOVA followed by Sidak's multiple comparisons test was used to perform comparisons of differentiated to the control cultures. For transcriptomic and proteomic data, *p*-values were corrected with Benjamini-Hochberg method and adjusted p-values <0.05 were considered statistically significant.

3. Results

3.1. Marked reduction of cell proliferation and increased ECM deposition upon ATDC5 cell differentiation

ATDC5 cells have been previously reported to produce a cartilage-like ECM composed of collagens and proteoglycans upon differentiation (Okita et al., 2023; Wilhelm et al., 2020; Tare et al., 2005). We used a standard protocol to differentiate ATDC5 cells with insulin, transferrin, sodium selenite and ascorbic acid (Altaf et al., 2006) for 4, 7, 14 or 21 days. As expected, visualization of deposited ECM using Alcian Blue and Sirius Red (Okita et al., 2023) revealed progressive matrix accumulation over time, more pronounced in cells treated with differentiation medium compared to cells in control medium (Fig. 1 A). Immunostaining for fibronectin, a protein binding to collagen fibrils and regulating fibril assembly (Paten et al., 2019; Engvall and Ruoslahti, 1977) at differentiation day 4 revealed the formation of an unorganized fibrillar ECM network (Fig. 1 B). In vivo, cellular differentiation of chondroprogenitor cells into first proliferating, then hypertrophic chondrocytes goes along with an initially increasing proliferation rate, followed by a termination of proliferation once cells reach hypertrophic stages of chondrogenesis (Goldring et al., 2006). We therefore tested the

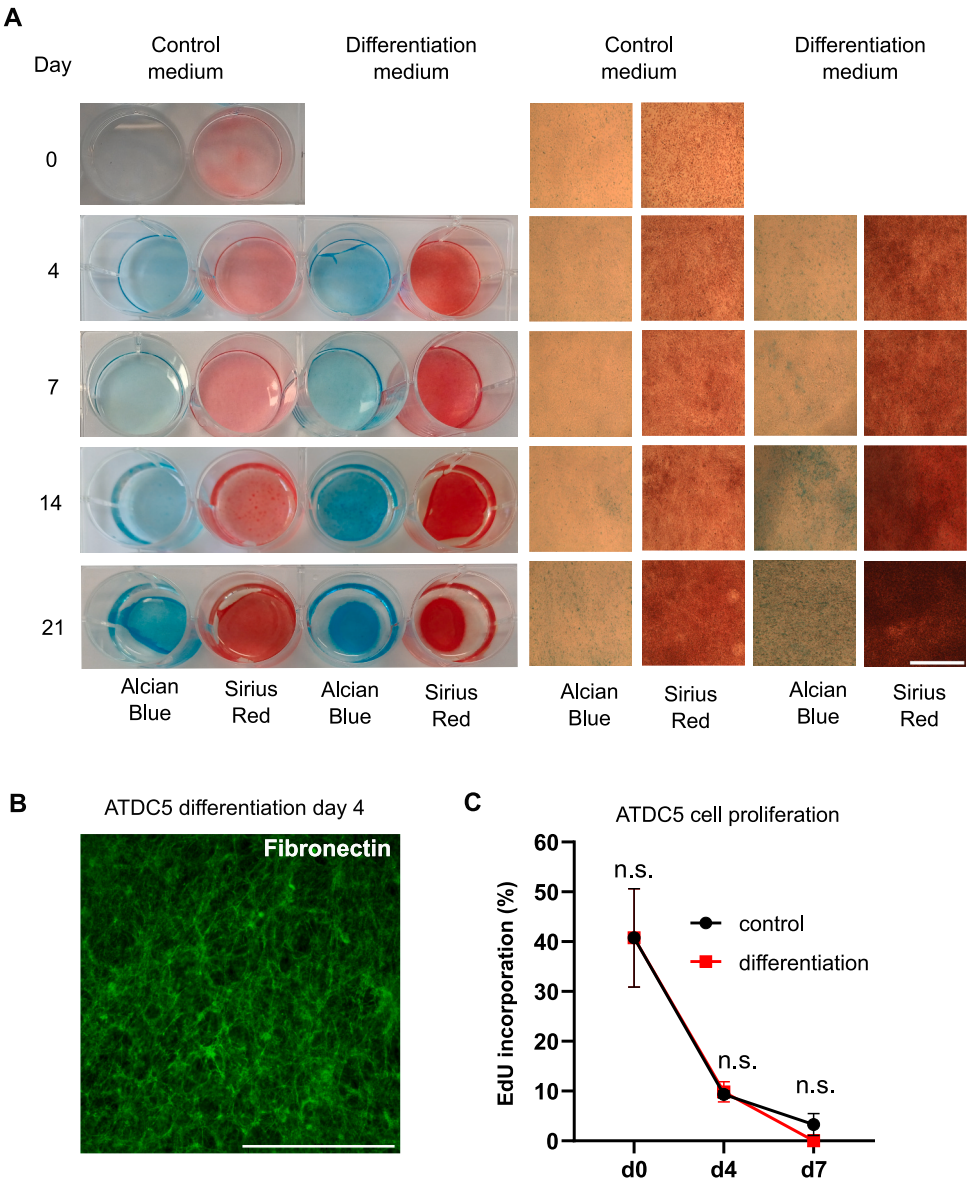

Fig. 1. ECM deposition and cell proliferation during ATDC5 differentiation
Cells were maintained in control medium (5% FCS) or differentiation medium (5% FCS, supplemented with 10 μg/ml insulin, 30 nM sodium selenite, 50 μg/ml ascorbic acid and 10 μg/ml transferrin). (A) Alcian Blue (marking proteoglycans) and Sirius Red (marking collagens) staining of cells maintained in control or differentiation medium at days 0, 4, 7, 14 and 21 of culture visualising progressive ECM accumulation over time. Scale bar: 1 mm. (B) Fibronectin staining of ATDC5-derived ECM after decellularization at day 4 of culture in differentiation medium. Scale bar: 100 μm. A representative image is shown. Images were taken using a Leica Thunder microscope. (C) To assess proliferation rates, the proportion of EdU (5-ethynyl-2′-deoxyuridine) positive nuclei was determined at day 0, 4 and 7 for cells maintained in control or differentiation medium. Data are presented as mean ± SD ($n = 3$). Two-way ANOVA followed by Sidak's multiple comparisons test was used to perform pairwise comparisons of differentiating cultures compared to control at each time point. *P*-values <0.05 were considered statistically significant.

impact of differentiation on ATDC5 cell proliferation which revealed observed a marked decrease in cell proliferation already by day 4 for both cells treated with control or with differentiation medium. By day 7, cell proliferation was undetectable for cells treated with differentiation medium and only minimal proliferation was observed for control medium cultures (Fig. 1 C). Potentially, as ATDC5 cells are derived from teratocarcinoma cells (Atsumi et al., 1990) with a fairly high proliferation rate already, increasing cell density over time could impact cell proliferation differently to what is observed upon in vivo chondrocyte differentiation. Other proliferation studies in ATDC5 cells have similarly shown that cell number and proliferation rate decrease over time (Temu et al., 2010; Hodax et al., 2019; Chen et al., 2005).

3.2. Transcriptional changes reflecting ATDC5 chondrogenic differentiation over time

ATDC5 cells are proposed to undergo a multistep chondrogenic differentiation, encompassing proliferative and hypertrophic stages (Newton et al., 2012; Tare et al., 2005; Shukunami et al., 1997; Shukunami et al., 1998) mimicking the process of endochondral bone formation. However, this conclusion is based mainly on studying expression of few marker genes, while genome-wide studies to investigate effects on the transcriptome are lacking. We therefore performed transcriptome analyses at day 0, 4, 7, 14 and 21 of cells cultured in differentiation medium.

Principal component analysis (PCA) showed distinct separation of samples by time point, with samples from day 14 and day 21 showing

particularly high similarity (Fig. S1). K-means clustering of normalized scaled counts identified five distinct gene clusters (Fig. 2 A). We subsequently used GO enrichment analysis to functionally characterize the genes within each cluster and to derive descriptive cluster annotations from most enriched GO terms. Cluster annotations are based on GO enrichment and are intended as descriptive summaries of dominant functional themes rather than definitive biological assignments. Cluster I (Translational initiation and uncharacterized genes), marked by genes with initially high but sharply declining expression after day 0, mainly consisted of predicted or poorly annotated genes. The remaining genes were predominantly associated with the GO term translation initiation (Fig. 2 B). Genes in cluster II (Immune response), the smallest cluster, showed a pronounced increase in expression shortly after the onset of differentiation at day 4 and were predominantly associated with the innate immune response (Fig. 2 C). Genes in cluster III, (ECM I) showed a modest increase between day 0 and 7 followed by a decrease until day 21 with GO term extracellular matrix organization (GO:0030198) found to be the most significant (Fig. 2 D), comprising 13 genes including *Abi3bp* and *Pdgfra*, which have known roles in early chondrogenesis (Bartoletti et al., 2020; Hodgkinson et al., 2013). Cluster IV (ECM II), was characterized by peak gene expression at day 14 and showing enrichment for genes related to cartilage development and ossification, encompassing key chondrocyte marker genes (Hissnauer et al., 2010; Sive et al., 2002) (*Acan*, *Col2a1*, *Hapln1*) (Fig. 2 E). Genes in clusters III and IV, both enriched for ECM and cartilage genes, showed lowest expression before culturing in differentiation medium, indicating that their expression is enhanced by the culture conditions. The largest cluster, cluster V (Angiogenic/metabolic response), showed a continuous increase in gene expression until day 21 (Fig. 2 F). GO analysis of all genes in clusters I-V revealed that genes that change most in expression during the differentiation process are associated with ECM and immunity linked GO terms (Fig. S2). Gene cluster lists and complete GO enrichment results are provided in Supplementary File S1.

To complement the clustering of normalized expression profiles, we further analyzed gene expression changes between consecutive sampling time points (Fig. 3 A-D, Supplementary File S2). When comparing the next later sampling timepoint to the previous sampling timepoint (day 4 to day 0, day 7 to day 4, day 14 to day 7 and day 21 to day 14), the highest number of differentially expressed genes was found between day 0 and day 4 (Fig. 3 A, E). As differentiation progressed, the number of differentially expressed genes between measurements decreased (Fig. 3 E). Comparison of day 4, day 7, day 14 and day 21 to day 0 directly revealed significantly increased expression of key chondrocyte genes such as *Col2a1*, *Acan*, and *Fmod* and the GO term "Extracellular Matrix organization" among the three most significant at all time points later than day 4 (Fig. 3 A, Fig. S3, Fig. S4, Supplementary File S3). While expression of these and other chondrocyte markers already increased between day 0 and day 4 (Fig. 3 A), the majority of genes showing

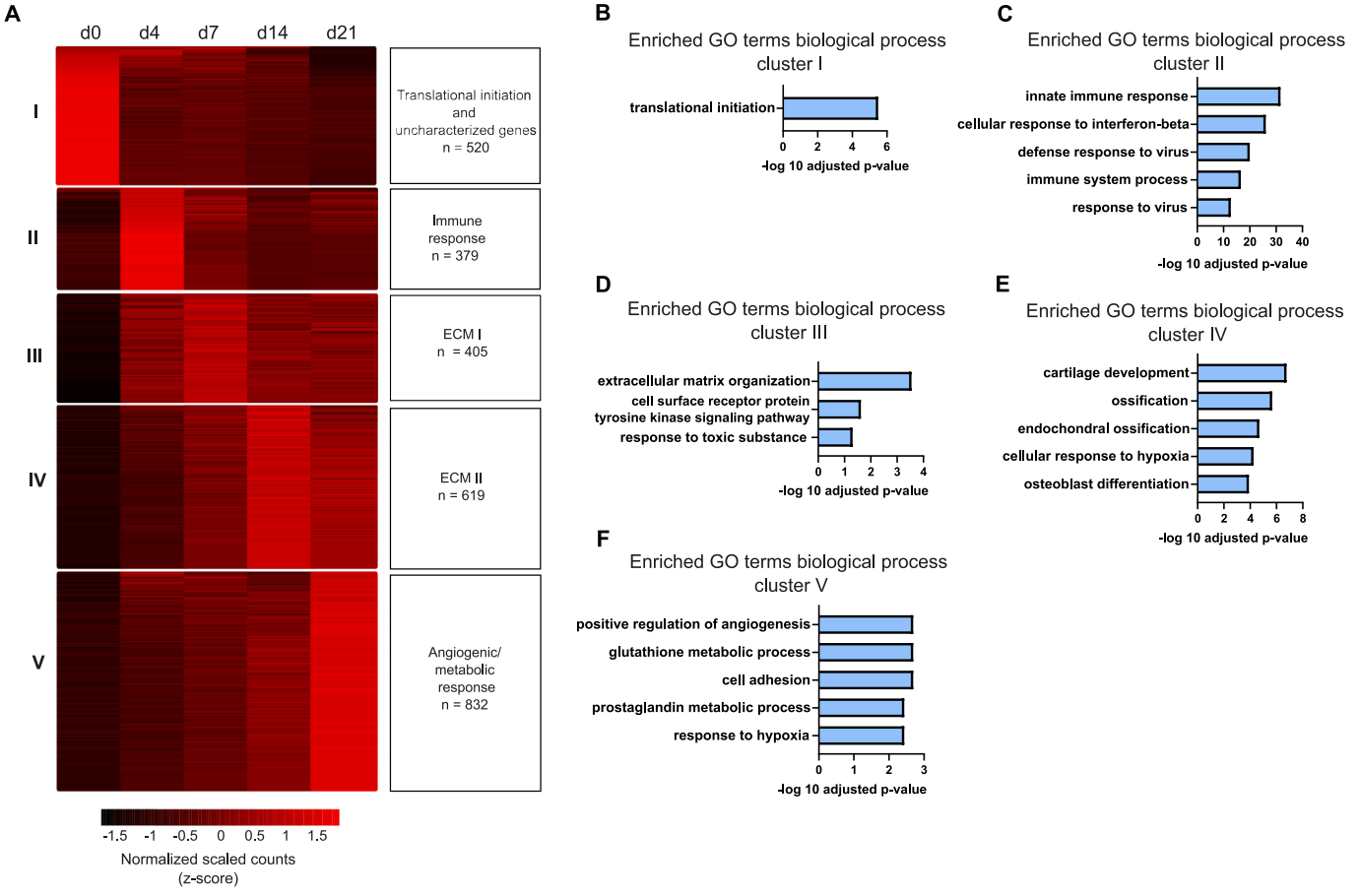

Fig. 2. Early immune response followed by ECM organization and lastly and angiogenic/metabolic response expression patterns over the course of ATDC5 differentiation.

(A) Differentially expressed genes (adjusted $p \leq 0.05$, $|\log2 \text{ fold change}| \geq 2$) were identified in ATDC5 cells maintained in differentiation medium at days 0, 4, 7, 14, and 21. RNA sequencing was performed using four biological replicates per time point. Differential expression was assessed using DESeq2 based on a two-sided Wald test with Benjamini–Hochberg correction. Genes were grouped into five clusters using k-means clustering. The heat map displays z-score scaled normalized expression values. (B-F) Gene ontology (GO) analysis for "biological process" (BP) of all genes in clusters I-V using DAVID Functional Annotation Tool. Top 5 or all identified GO terms are displayed. For analysis of cluster I (B), genes that were no annotated (predicted genes) were excluded. Full list of genes and GO analysis per cluster are listed in Supplementary File S1.

increased expression at day 4 were not related to chondrocyte differentiation but rather associated with immune response as revealed by GO analysis (Fig. S5 B, Supplementary File S3). Concurrently, genes related to cell division decreased in expression (Fig. S5 A). The expression of chondrocyte differentiation, ECM- and ossification-related genes increased over time, most prominently between day 7 and day 14, as exemplified by increased expression of *Col10a1*, *Hapln1*, and *Comp* (Fig. 3 C). This was accompanied by strong enrichment of GO terms related to cartilage development and ossification (Fig. S5).

Representative chondrocyte differentiation and ECM genes (Lawrence et al., 2025; Sebastian et al., 2021) including collagens, proteoglycans, and transcription factors, showed a gradual increase in expression from day 0, peaking at day 14 (Fig. 3 F) with only few exceptions. *Col2a1*, a marker of the proliferative chondrocyte phase (Zhao et al., 1997), was representative of this general expression pattern (Fig. S1 B). In contrast, expression of *Col10a1*, a marker of hypertrophic differentiation (Gu et al., 2014), increased only modestly during early differentiation but rose sharply from day 7 onwards and continued to increase beyond day 14 (Fig. S1 C). Similarly, *Spp1*, encoding the osteogenic glycoprotein osteopontin involved in bone mineralization (Holm et al., 2014), reached its highest expression level at day 21. *Ucma*, encoding a negative regulator of osteogenesis usually expressed in early chondrogenesis (Surmann-Schmitt et al., 2008), showed highest gene expression at day 7. Interestingly, *Sox9* and *Runx2*, master transcription factors of chondrogenic (Akiyama et al., 2002; Lefebvre and Dvir-Ginzberg, 2017) and osteogenic differentiation (Ziros et al., 2008), reached their highest expression levels at day 14, although their overall expression increased only modestly over the course of differentiation (Fig. 3 F, Fig. S1 D). The overall stable expression of Sox9 is in accordance with previous ATDC5 studies (Altaf et al., 2006; Temu et al., 2010; Chen et al., 2005; Caron et al., 2021; Dong et al., 2021). In contrast, studies have reported either a progressive increase in Runx2 expression over time (Altaf et al., 2006; Temu et al., 2010) or a transient increase followed by a decline (Chen et al., 2005; Dong et al., 2021). Published in vivo data suggests that Sox9 expression is typically declining during hypertrophic differentiation, however Runx2 expression has been reported to increase upon chondrocyte prehypertrophy (Goldring et al., 2006; Leung et al., 2011; Kim et al., 1999).

When comparing the intervals between day 7 vs. day 4, as well as between day 14 vs. day 7, immunity-related genes showed a decrease in expression, as indicated by GO analysis (Fig. S5 C, E). This is consistent with the expression pattern observed for cluster II, which could indicate a stress effect resulting from addition of differentiation medium and cells reaching full confluency.

3.3. Dissection of the ATDC5-derived cartilage-like proteome

To investigate the composition of the cartilage-like matrix generated by ATDC5 cells over time upon differentiation, we performed quantitative proteomics analyses. Samples collected after 4, 7, 14 or 21 days of differentiation were decellularized while on day 0, cells were retained.

Principal component analysis revealed clear clustering of samples by time points (Fig. 4 B), with day 0 samples clearly separated from all other timepoints. In addition, while day 4, 7 and 14 samples clustered close together, day 21 samples appeared distinct although comparatively few ECM proteins showed differential expression between day 14 and day 21 (Fig. 4 F).

A protein was considered identified if it was detected in at least two out of four biological replicates at any time point. This led to identification of 8316 proteins across all samples, further referred to as the ATDC5 proteome (Supplementary file S4). To specifically and systematically analyze expression patterns of ECM-related proteins within the dataset, we next assessed which of the identified proteins overlapped with those annotated in the Gene Ontology term “extracellular matrix” (GO:0031012). 216 of the 8316 identified proteins were annotated in GO:0031012 (Table 1), of which 161 proteins (74.5%) were consistently identified at all time points (Fig. 4 A), including collagens (COL2A1, COL6A1, COL11A1), proteoglycans (CSPG4, BGN, HSPG2), glycoproteins (EMILIN1, MATN2, SMOC1) and ECM-modifying enzymes (ADAMTS5, HTRA1, LOX). 36 proteins were expressed at all time points between day 4 and day 21 after differentiation onset but not day 0, indicating that their expression is induced by the culturing conditions (Fig. 4 A). These included aggrecan core protein (ACAN), forming the core of the most abundant proteoglycan in cartilage (Horkay et al., 2017; Kiani et al., 2002), and hyaluronan and proteoglycan link protein 1 (HAPLN1), a key structural component of the cartilage matrix (Neame and Barry, 1993). Several other collagens and proteoglycans were also newly detected during this period including ASPN, DCN, FMOD and LUM, in accordance with their increased expression on gene level comparing day 4 vs. day 0 (Fig. 3 A). 19 of 216 ECM proteins were detected only at three or fewer time points (Fig. 4 A, Table 1). Beyond day 4, expression of proteins annotated in GO:0031012 “extracellular matrix”, increased almost exclusively over time, with very few exceptions (Fig. 4 D-F). Comparison of ECM protein expression at days 4, 7, 14 and 21 relative to day 0 revealed a consistent expression pattern, with a high number of proteins increasing in expression and a small subset of proteins showing lower abundance over time, including cathepsin proteases (CTSZ, CTSB, CTSL, CTSD), which are found intra- and extracellularly (Vidak et al., 2019). Across all time points, HTRA1, POSTN, BGN, NID2, COL12A1 and MMP19 were among the most significant increasingly expressed ECM proteins (Fig. 4 C, Fig. S6). Notably, COL10A1, was only identified at day 14 and day 21, consistent with its pronounced increase in gene expression observed at day 14 in transcriptomic analysis (Fig. S1 C).

To assess whether ECM protein expression followed specific temporal patterns, representative proteins were visualized in heatmaps (Fig. 5). The majority of proteins reached peak expression at either day 14 or day 21, consistent of a progressive accumulation of secreted proteins over time. Proteins were grouped into functional categories: collagens, proteoglycans, glycoproteins, ECM receptors, and ECM-modifying enzymes, thereby encompassing the most relevant ECM components. Collectively, the heatmaps show that the majority of ECM proteins increase steadily over time, independent of functional category. For a comprehensive heatmap including all 216 ECM proteins identified in our dataset see Fig. S7.

3.4. Concordant temporal patterns in transcriptomic and proteomic analyses

In general, transcriptomic and proteomic analyses revealed similar temporal trends. In both datasets, ECM-associated genes and ECM proteins increased in expression following the onset of differentiation, with strong induction already observed at day 4 compared to day 0 (Fig. 3 A, Fig. 4 C). In both analyses, the main increase in ECM genes or proteins occurred between day 7 and 14. In the transcriptomic analysis, expression levels of ECM related genes declined again after day 14, while in the proteomic dataset only few ECM proteins showed significant decreases or increases in abundance between day 14 and 21, indicating limited changes in ECM protein abundances despite changes in gene expression. A direct comparison of significantly regulated ECM-associated genes and proteins (GO:0031012) showing the same direction of change between consecutive sampling time points confirmed this overall agreement between transcriptomic and proteomic analyses. The largest overlap was observed between day 0 and day 4, with 33 ECM genes and proteins showing concordant increase in expression (Table 2), of which 9 were collagens, including the highly abundant early collagen COL2A1. Smaller overlaps of genes and proteins with increased expression were observed for the comparisons day 7 versus day 4 (14 genes/proteins) and day 14 versus day 7 (12 genes/proteins), including two major ECM components ACAN and HAPLN1, as well as small proteoglycans LUM, DCN and FMOD in both intervals. Between day 21 and day 14 no shared significantly regulated ECM genes and proteins were identified.

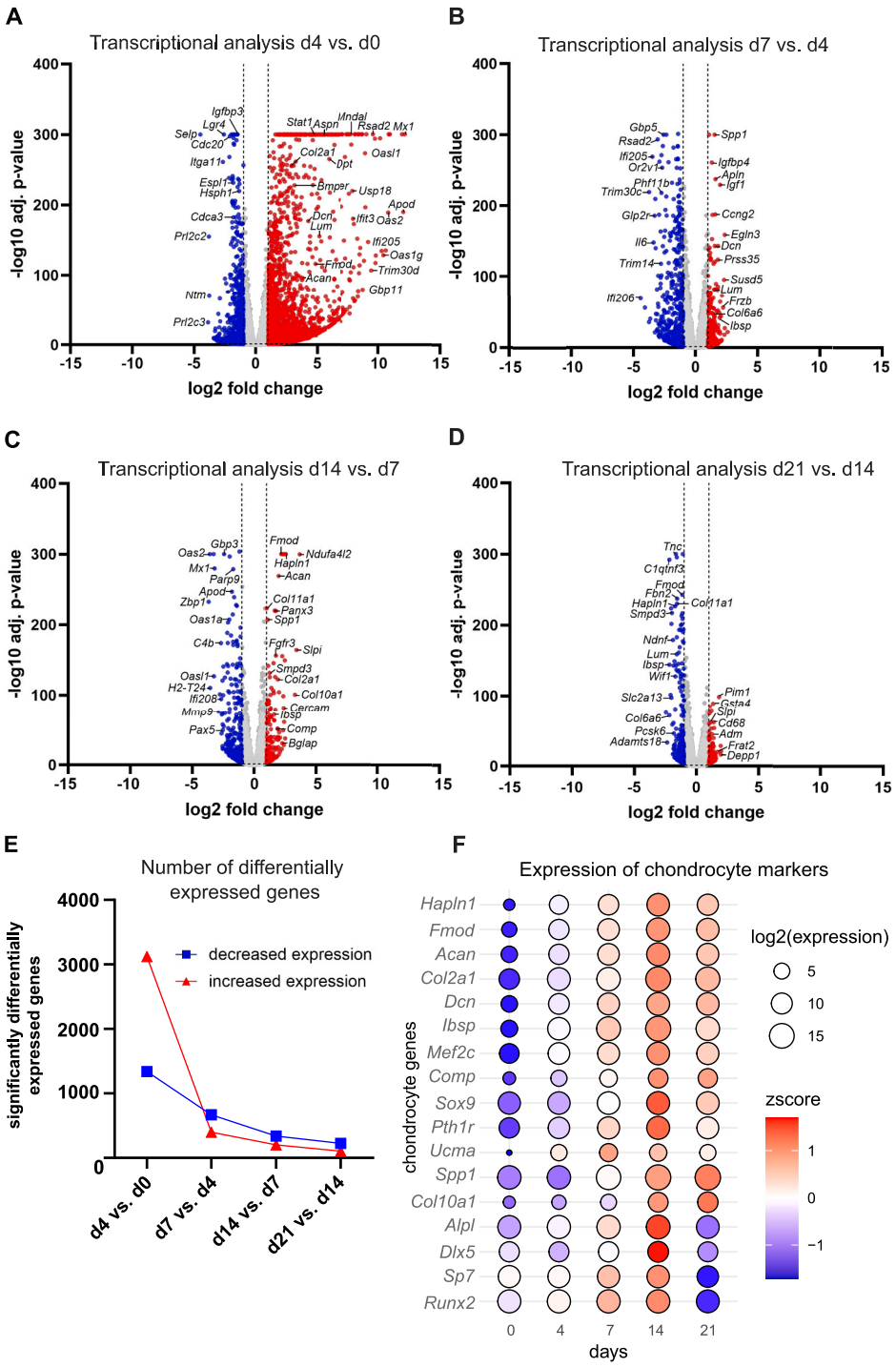

Fig. 3. Increasing expression of key chondrocyte marker genes upon differentiation peaking at day 14.
(A-D) Volcano plots display differential gene expression between consecutive time points based on RNA-seq data, revealing significant increase in expression of chondrocyte differentiation genes such as *Col2a1*, *Acan* and *Fmod*. The x-axis indicates log2 fold change, the y-axis shows the −log10 adjusted *p*-value. For visualization purposes, −log10 adjusted *p*-values were capped at 300. Genes were color-coded according to log2fold change thresholds of ±1. RNA sequencing was performed using four biological replicates per time point. Differential expression was assessed using DESeq2 based on a two-sided Wald test with Benjamini–Hochberg correction; genes with adjusted $p \leq 0.05$ were considered significantly differentially expressed. (E) Number of differentially expressed genes with increasing or decreasing expression during sampling intervals, showing overall decreasing numbers of differentially expressed genes as differentiation progressed. (F) Dot plot displaying the expression of selected chondrocyte marker genes across the indicated time points with peak expression at day 14. Dot size represents log2-transformed expression values, while color intensity indicates z-score-scaled expression levels for each gene. Expression values are derived from DESeq2-normalized RNA-seq counts.

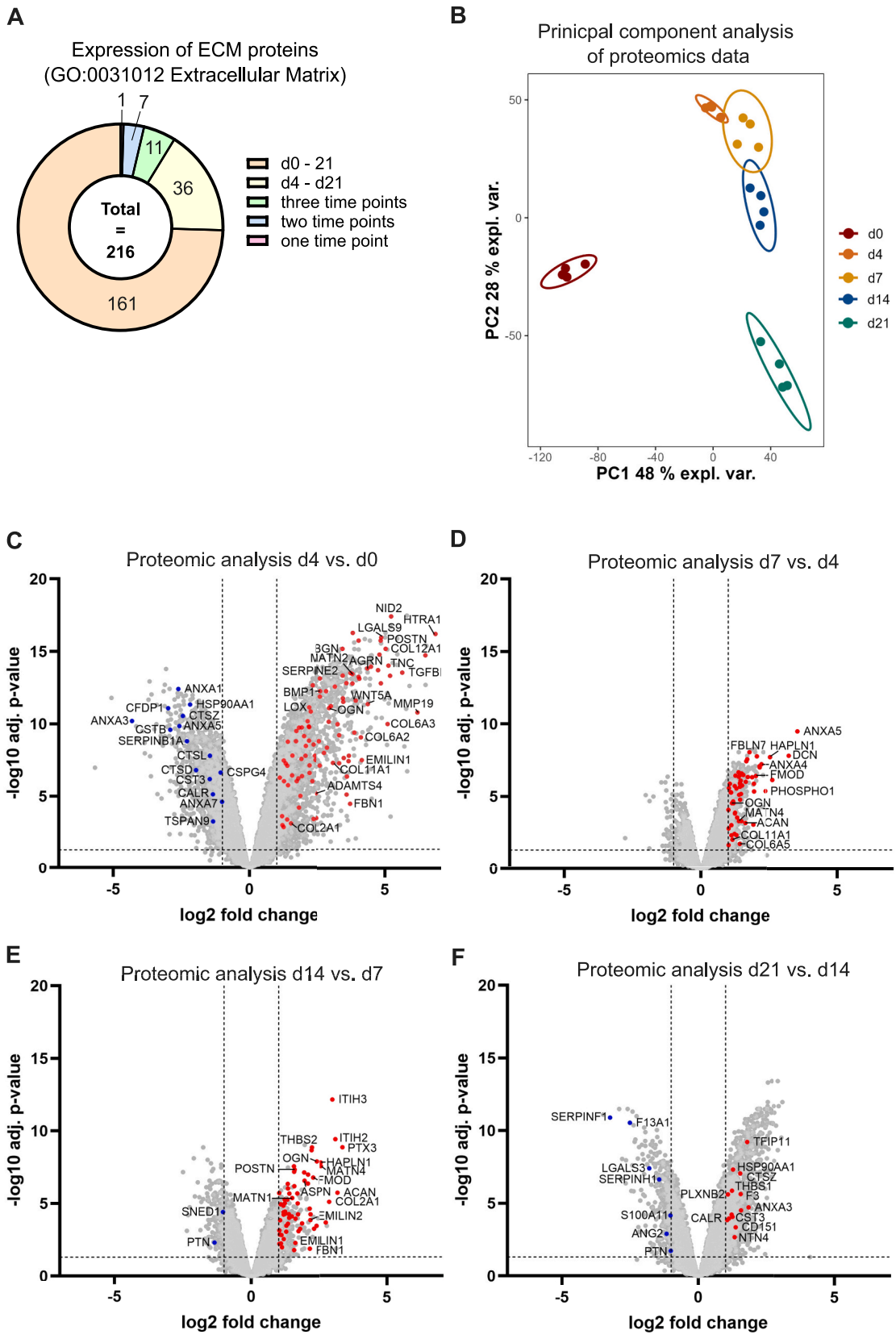

(caption on next page)

Fig. 4. Proteomics analyses reveal increasing expression of cartilage ECM proteins in ATDC5-derived ECM over time.
Proteomic analyses were performed using four replicates per time point. Differential protein expression was assessed using limma, and p-values were corrected for multiple testing using the Benjamini–Hochberg method. Proteins with adjusted $p \leq 0.05$ were considered significantly differentially expressed. (A) Donut plot illustrating the number of ECM proteins, annotated in GO:0031012 ECM, that were detected throughout the experiment, at day 4, 7, 14 and 21, or at three or fewer time points. A total of 161 proteins were consistently detected at all time points, whereas 36 proteins were detected from day 4 onwards (including day 4) but not at day 0. Only few proteins were detected at three or fewer time points. For a complete list of all identified proteins and the time points at which they were detected, refer to Table 1. (B) Principal component analysis (PCA) of proteomic samples based on log_2-transformed and median-normalized protein intensities, showing clustering of samples by time point. PC1 and PC2 explain 48% and 28% of total variance. Samples are color-coded according to differentiation time (day 0, 4, 7,14 or 21). (C-F) Volcano plots display differential protein expression between consecutive time points, illustrating a progressive increase in ECM protein expression at each successive time interval. ECM proteins were color-coded according to adjusted $p \leq 0.05$ and log2fold change thresholds of ± 1. The x-axis indicates log2 fold change, the y-axis shows the $-$log10 adjusted p-value. Proteins not annotated in GO:0031012 ECM are displayed in grey.

Table 1
ECM proteins detected in ATDC5-derived ECM. Proteins annotated to GO:0031012 (Extracellular matrix) identified in this study and ordered by detection time points.

d0 ∩ d4 ∩ d7 ∩ d14 ∩ d21	d4 ∩ d7 ∩ d14 ∩ d21	d4 ∩ d7 ∩ d14	d7 ∩ d14 ∩ d21	d0 ∩ d14 ∩ d21	d0 ∩ d7	d4 ∩ d7	d7 ∩ d14	d14 ∩ d21	d21
ADAM10, ADAMTS1, ADAMTS2, ADAMTS4, ADAMTS5, ADAMTSL4, AGRN, AHSG, ALB, ALPL, ANGPTL2, ANXA1, ANXA11, ANXA2, ANXA3, ANXA4, ANXA5, ANXA6, ANXA7, BGN, BMP1, CALR, CASK, CCDC80, CCN1, CCN2, CCN4, CCN5, CFDP1, COL11A1, COL12A1, COL15A1, COL16A1, COL1A1, COL1A2, COL2A1, COL3A1, COL4A1, COL4A5, COL5A1, COL5A2, COL6A1, COL6A2, COL6A3, COLEC12, CSPG4, CST3, CSTB, CTHRC1, CTSB, CTSD, CTSL, CTSZ, DAG1, DLG1, ECM1, EFEMP2, EMILIN1, EMILIN2, F13A1, F2, F3, FAM20B, FBLN1, FBLN2, FBN1, FBN2, FGB, FGG, FN1, GFOD2, GLG1, GPC1, GPC4, GSTO1, HCFC1, SD17B12, HSP90AA1, HSPG2, HTRA1,IGF2, IGFBP6, ITGB1, ITIH2, ITIH3, ITIH4, LAMA4, LAMB1, LAMB2, LAMC1, LGALS1, LGALS3, LGALS9, LGALSL, LMAN1, LOX, LOXL1, LTBP1, LTBP3, MATN2, MFGE8, MGP, MMP14, MMP2, NDNF, NGLY1, NID1, NID2, NTN1, OGN, P3H1, PCOLCE2, PHOSPHO1, PLG, PLOD1, PLOD2, PLOD3, PLXNB2,POSTN, PRG4, PTN, PXDN, RPSA, RUNX1, S100A10, S100A11, S100A13, S100A6, SEMA3C, SERAC1, SERPINB1A, SERPINC1, SERPINE1, SERPINE2, SERPINF1, SERPINH1, SMC3, SMOC1, SMOC2, SNED1, SOD3, SPARC, TFIP11, TGFB1, TGFB2, TGFBI, TGM2, THBS1, THBS2, THBS3, TIMP1, TIMP2, TIMP3, TINAGL1, TNC, TNFRSF11B, TNN, TSPAN9, VCAN, VWA5A, WNT5A	ABI3BP, ACAN, ADAMTSL1, ANG2, ASPN, BMPER, COL11A2, COL18A1, COL4A2, COL6A5, COL6A6, COL8A1, DCN, DPT, ECM2, FBLN5, FBLN7, FGL2, FMOD, HAPLN1, INS1, LAMA5, LUM, MAMDC2, MATN1, MMP11, MMP19, NPNT, NTN3, OMD, PRELP, PTX3, SRPX2, THSD4, VTN, WNT5B	EFEMP1 HMCN1 IL16 SVEP1	ADAMTS3 COL14A1 COL6A1 LTBP4 MATN4 MFAP2	CD151	PLXNA2	SSC5D	CLEC3B	COL10A1 COL9A1 NTN4 SPON2	ITGA6

Table 1: ECM proteins (GO:0031012) detected at respective time points.

Concordant decrease in expression was only observed for SERPINB1A between day 0 and day 4, but not at any other time points, probably reflecting enhanced ECM production and accumulation during ATDC5 differentiation, while matrix breakdown appears to be less prominent.

3.5. ATDC5-derived ECM contains a broader spectrum of ECM proteins than previously reported

ECM proteome composition over time during ATDC5 differentiation has been unclear prior to this study. Therefore, we aimed to systematically investigate the ATDC5-derived ECM proteome and place it in the context of the only other existing dataset previously published by Wilhelm et al. (2020). To do this, we first compared both our dataset and that of Wilhelm et al. to proteins annotated in the Gene Ontology term "extracellular matrix" (GO:0031012), as this provides a well-established and widely accepted framework for the functional classification of proteins. Moreover, we compared both datasets to the full list of proteins in the Matrisome database (Shao et al., 2023) which provides a more comprehensive reference list of ECM components and is derived from two independent proteomic studies of murine cartilage (Georgieva et al., 2020; Bubb et al., 2021).

The comparison of our and Wilhelm et al.'s dataset to GO:0031012 revealed 62 ECM proteins commonly detected in both studies (Fig. 6 A, Supplementary File S5), including the highly abundant fibrillar collagen COL2A1, as well as less abundant collagens including COL6A1, COL6A2, COL11A1, COL11A2 and COL10A1 (Alcaide-Ruggiero et al., 2021), the main cartilage proteoglycan aggrecan as well as several small leucine-rich proteoglycans (SLRPs), glycoproteins and ECM-modifying

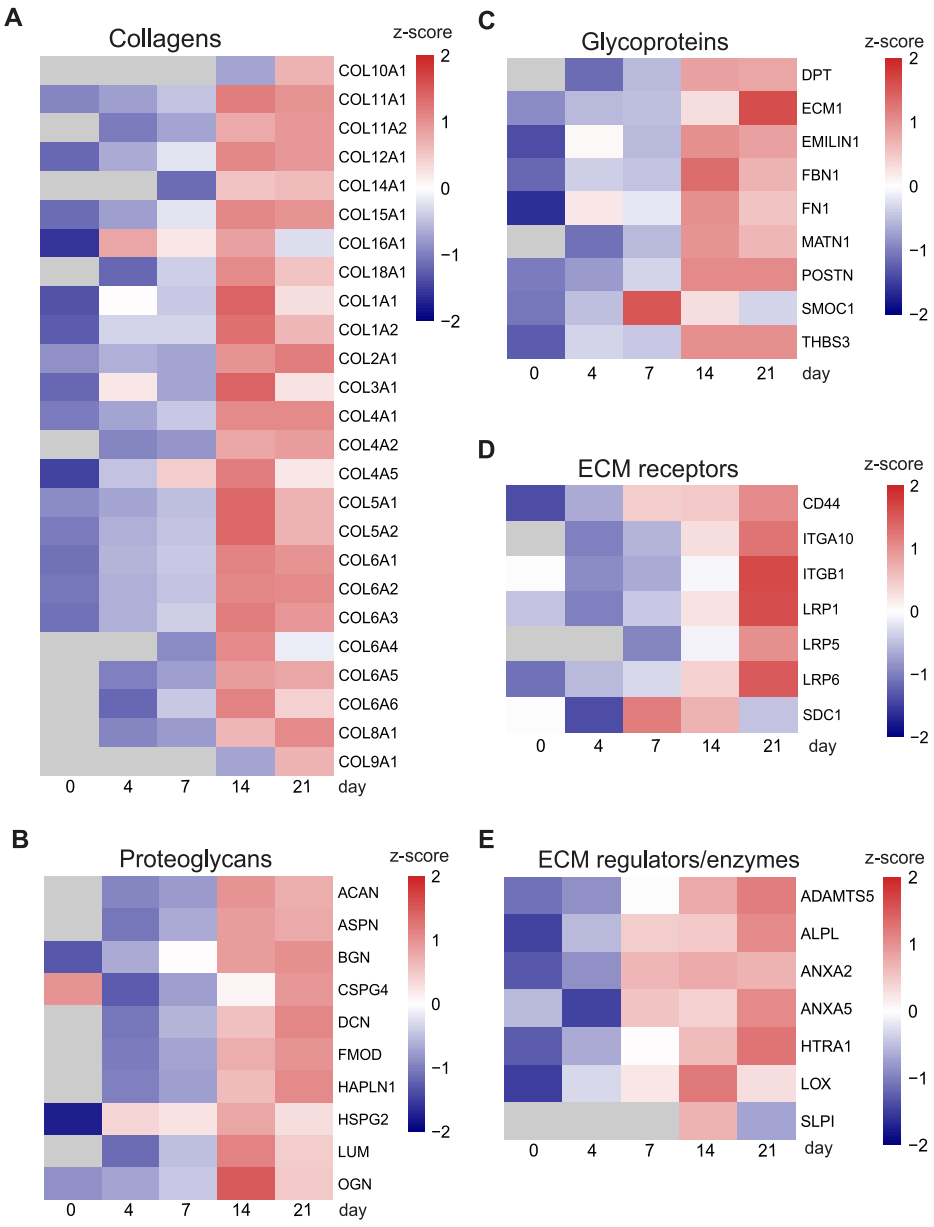

Fig. 5. Consistent increase in ECM protein abundance across functional categories during ATDC5 cell differentiation.
(A-E) Heatmaps of representative ECM proteins across functional categories (collagens, proteoglycans, Glycoproteins, ECM receptors, ECM regulators/enzymes). Proteomic analyses were performed using four replicates per time point. Selected proteins from different ECM categories are shown. Normalized expression values were derived from the log2 intensities (expression matrix) and mean values were calculated across four replicates per time point. Expression values are scaled per protein (z-score) to illustrate relative abundance patterns across timepoints. Most proteins show low expression at the beginning of differentiation, with peak expression observed at day 14 or 21, with only a few exceptions.

enzymes, reflecting the structural diversity of the cartilage ECM captured in both datasets. Conversely, we could not detect six ECM proteins reported by Wilhelm et al. (COL20A1, COL23A1, COL27A1, COL4A3 and COL4A4). Notably, we detected 154 ECM proteins not previously reported by Wilhelm et al. (Fig. 6 A, Supplementary File S5). These proteins spanned a wide range of ECM categories, including minor collagens, proteoglycans, annexins, matrilins, laminin chains, microfibril-associated components, secreted signalling proteins and ECM-remodeling enzymes such as ADAMTS family members and matrix-metalloproteinases (MMPs).

Next, we compared our and Wilhelm et al.'s dataset to a list of murine cartilage proteins annotated in the Matrisome Database (Shao et al., 2023) (Fig. 6 B). Of 68 proteins that were detected in both our and Wilhelm et al.'s study and are listed in the Matrisome Database, 12 proteins were not annotated in GO:0031012 “ECM” (AEBP1, CLEC11A, CX3CL1, FSTL1, IGFBP5, IGSF10, LOXL4, P4HA1, P4HA2, PCOLCE, SLPI, SPP1) (Fig. 6 B, Fig. S8 A, Supplementary File S5). Further, this comparison revealed 189 proteins only identified in our dataset but not Wilhelm et al.ś study that were also detected in native cartilage, and further 68 proteins that were detected in both our study and by Wilhelm et al. (Fig. 6 B, Supplementary File S5). Among these 189 uniquely identified proteins, those that were not annotated in GO term “extracellular matrix”, encompassed multiple ECM classes including proteoglycans, ECM remodeling enzymes and regulators, as well as secreted signalling factors (Fig. 6 B, Fig. S8 A). Comparison of Wilhelm et al.'s dataset with the Matrisome database identified five further ECM proteins (HPX, IBSP, IGFBP2, PCSK5, VWA5B2) that were not detected in our dataset (Fig. S8 A). GO analysis of proteins that were neither

Table 2
List of shared significantly regulated ECM genes and proteins annotated in GO:0031012 with concordant increase or decrease in expression between consecutive sampling time points.

Comparison	day 4 vs. day 0	day 7 vs. day 4	day 14 vs. day 7	day 21 vs. day 14
Shared significantly regulated ECM genes/proteins with concordant increase in expression	Adamts1 Adamts2 Adamts4 Agrn Col11a1 Col11a2 Col1a1 Col2a1 Col3a1 Col4a1 Col4a5 Col6a3 Col8a1 F13a1 Fbln5 Fbn1 Htra1 Itih2 Lama4 Lamb1 Lgals9 Loxl1 Mmp19 Nid1 Nid2 Ntn1 Ogn Phospho1 Tgfb2 Tgm2 Tnc Vcan Wnt5a	Acan Col6a5 Col6a6 Dcn F13a1 Fbln7 Fmod Hapln1 Lama5 Lum Matn4 Phospho1 Prelp Thsd4	Acan Ccn2 Col11a1 Col11a2 Col2a1 Dcn F13a1 Fmod Hapln1 Lgals3 Lum Matn4	None
Shared significantly regulated ECM genes/proteins with concordant decrease in expression	Serpinb1a	None	None	None

identified in our nor Wilhelm et al.́s dataset but listed in GO:0031012 or Matrisome database (593 proteins, Fig. S8 A) revealed predominantly proteins associated with GO terms “ECM organization”, “proteolysis” and “collagen catabolic process” (Fig. S8 B, Supplementary File S6).

Overall, our analysis has revealed an extended set of ECM proteins in ATDC5 produced matrix, capturing components that were not previously reported and highlighting the ECM complexity ATDC5-derived ECM. The newly detected ECM proteins each fulfill specific functions and contribute to extracellular matrix assembly and homeostasis, for example as structural components, ECM remodeling enzymes, and signalling proteins that mediate matrix-related signalling. Further, mutations in several of the newly detected proteins such as in FBN1, MATN3, GPC6 and LTBP1 are associated with genetic skeletal diseases (Unger et al., 2023), underscoring the biological relevance of the detected proteins.

4. Discussion

The ATDC5 model system is widely used to study chondrogenic differentiation. Most previous studies relied on targeted approaches to monitor chondrocyte differentiation (Okita et al., 2023; Newton et al., 2012; Yuan et al., 2022; Shukunami et al., 1997; Chen et al., 2006), such as qPCR of a low number of selected chondrocyte marker genes, while only very few studies used comprehensive RNAseq (Caron et al., 2021; Farcasanu et al., 2025) or ECM proteomic (Wilhelm et al., 2020) approaches. Thus, there was need for an unbiased genome-wide characterization of gene expression among different timepoints ATDC5 in vitro differentiation as well as characterization of the produced ECM. In this study, we combined time-resolved RNA sequencing with ECM proteomics to provide an integrated view of transcriptional dynamics and matrix deposition during ATDC5 differentiation. Although ATDC5 cells do not fully reproduce the distinct sequential stages of chondrocyte maturation observed in vivo, they capture key temporal molecular features of chondrogenesis, including induction of chondrogenic markers, progressive extracellular matrix deposition, and late expression of hypertrophic markers such as Col10a1. This supports their use as a simplified model to study fundamental aspects of chondrocyte differentiation. The gained insights into ATDC5 differentiation provide a temporal reference framework for future mechanistic studies that could involve gene edited cells in order to investigate chondrogenesis in genetic skeletal diseases or may investigate treatment of osteoarthritis, before moving to more complex models.

Consistent with previous studies (Okita et al., 2023; Newton et al., 2012; Tare et al., 2005; Challa et al., 2010), staining with Alcian Blue and Sirius Red revealed progressive extracellular matrix deposition over time. Interestingly, proliferative activity decreased rapidly after day 0, when cells were confluent, similarly in both control and differentiating ATDC5 cultures. This suggests that the observed decrease in proliferation is primarily driven by contact inhibition associated with high cell density rather than chondrogenic differentiation. This represents an important limitation of the model as in vivo differentiating chondrocytes are generally assumed to pass through a proliferative phase during early chondrogenesis, characterized by increased proliferative activity under physiological conditions (Goldring et al., 2006). Importantly, we cannot exclude that high cell density-associated effects influence the transcriptomic profile and may also impact downstream protein abundance, as suggested by previous studies (LeBlanc et al., 2022; Kim et al., 2017). Another important limitation is the absence of mechanical loading or stimulation, which plays an important role in regulating chondrogenic differentiation in vivo (Jia et al., 2023).

At the structural level, in agreement with previously published TEM images of ATDC5-derived ECM (Newton et al., 2012), fibronectin staining indicated a largely unorganized fibrillar ECM in ATDC5 cultures, which may reflect the constraints of a monolayer culture system and contrasts with the mostly ordered collagen architecture found in native cartilage (Gottardi et al., 2016; Moger et al., 2007). This highlights an important difference between ATDC5-derived ECM and in vivo cartilage.

Apart from the study by Chen et al. (2005), which analyzed the expression of 104 selected chondrocyte-associated genes using real-time RT-PCR, most transcriptional investigations of ATDC5 cells have most commonly focussed on *Col2a1*, *Col10a1* and *Sox9*. Consistent with these reports (Altaf et al., 2006; Temu et al., 2010; Hodax et al., 2019; Chen et al., 2005; Caron et al., 2021; Dong et al., 2021), our data confirm a strong and early induction of *Col2a1* expression, delayed expression of *Col10a1* and comparatively stable expression levels of *Sox9* and *Runx2* over the course of differentiation. This is of note, as SOX9 is highly, but not exclusively (Lawrence et al., 2025; Molin et al., 2024), expressed in proliferative chondrocytes (Zhao et al., 1997; Leung et al., 2011), whereas RUNX2 expression is linked to hypertrophic chondrocyte differentiation (Kim et al., 1999). This indicates a cell identity change towards a chondrogenic pattern over time, however ATDC5 in vitro differentiation stages do not exactly match known chondrocyte differentiation stages in vivo.

Beyond selected differentiation markers, unbiased transcriptomic analysis revealed that a broad set of chondrocyte- and ECM-related genes increased continuously over time until day 14. Additionally, few genes such as *Col10a1* and *Spp1*, showed peak expression at day 21, demonstrating that ATDC5 cells may have reached a hypertrophic-like stage at this later time points.

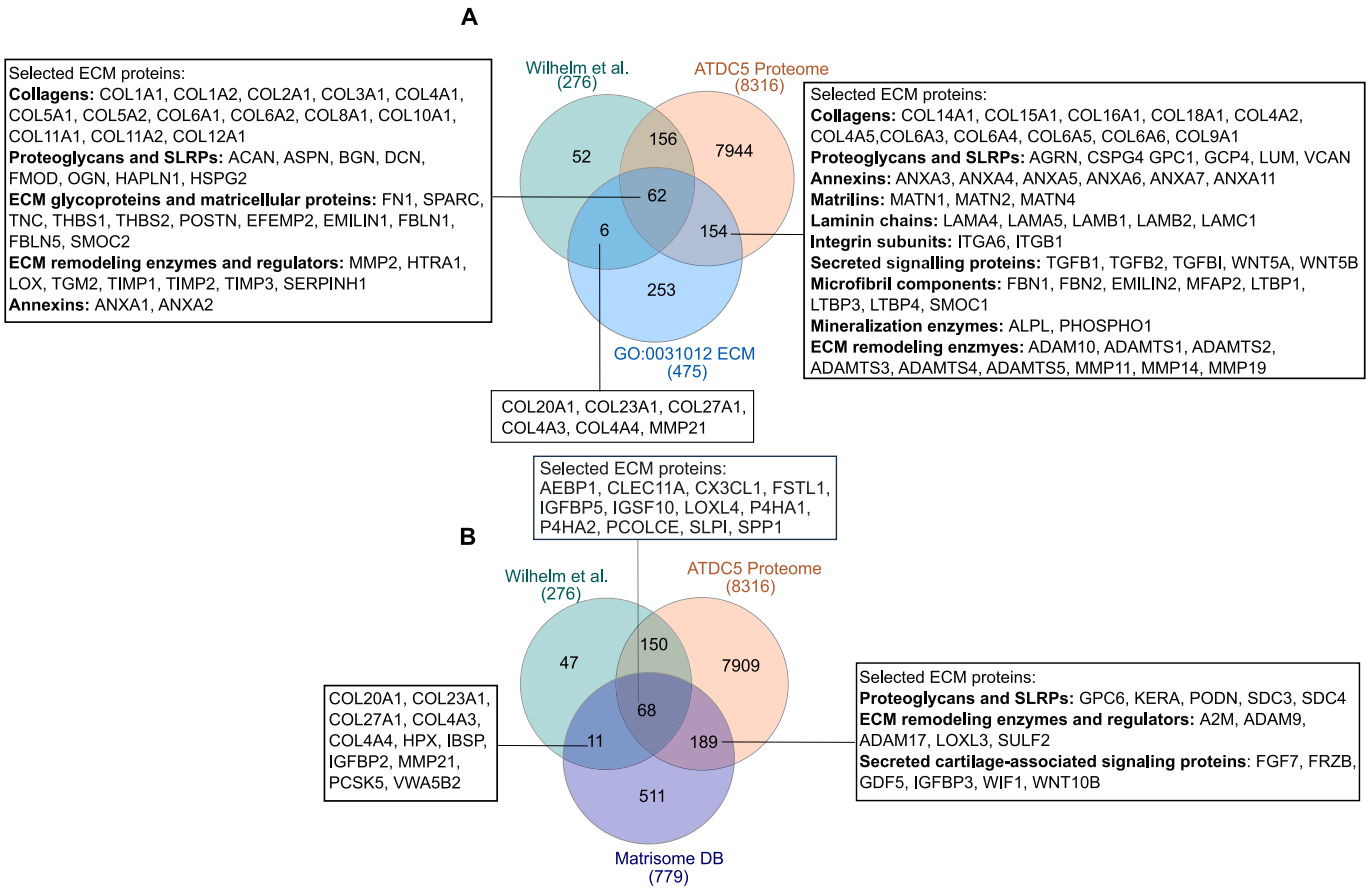

Fig. 6. Comparison of detected proteins reveals previously not reported ECM proteins in ATDC5 derived ECM.
(A) Venn diagram illustrating overlap of proteins identified in our study (ATDC5 proteome, $n = 4$ replicates per time point), Wilhelm et al.'s study and proteins annotated in the GO term "extracellular matrix" (GO:0031012), revealing 154 ECM proteins from numerous functional groups, that were not previously detected in ATDC5 cells (B) Venn diagram illustrating overlap of proteins identified in our study (ATDC5 proteome), Wilhelm et al.'s study and the Matrisome database, uncovering 189 ECM proteins not previously reported in ATDC5 cells. GO:0031012 and the Matrisome database were used as functional annotation frameworks for ECM classification.

While the model captures temporal aspects in gene expression related to chondrocyte differentiation, one might have expected clearer separation of ECM gene clusters corresponding to distinct phases of chondrogenesis (Wang et al., 2004; Tchetina et al., 2003). However, a detailed division between proliferative and hypertrophic stages is not apparent in our data. Potentially, this could be better resolved by investigating more time points. Heterogeneity in the differentiation stage of individual cells, as reflected by nodule formation (Shukunami et al., 1997) could also play a role.

Moreover, we identified a small transient gene cluster peaking at day 4 that was enriched for immune-associated Gene Ontology terms. Likewise, Farcasanu et al. (2025) identified immune-associated Gene Ontology terms in their ATDC5 transcriptomic analysis, using the same differentiation protocol as in our study. This suggests that the observed transcriptional pattern may represent a reproducible adaptive response of the in vitro culture system rather than a clearly stage-defining chondrogenic program. Such an adaptive response may be triggered by the altered culture conditions at differentiation onset, including insulin stimulation (Makhijani et al., 2023) as well as cell-intrinsic stress responses induced by metabolic constraints and hypoxia in over-confluent cultures (Luo et al., 2022; Cummins et al., 2006). However, although not classically associated with chondrogenesis, the activation of innate immune-related gene programs has also rarely been reported during human chondrogenesis (Liang et al., 2022; Zhou et al., 2019) so that the biological significance of the activation of immune-related genes during chondrogenesis remains to be determined.

Further, the subsequent decline in ECM-related gene expression after day 14, coinciding with increased expression of genes associated with angiogenesis, hypoxia and glutathione metabolism, suggests the activation of transcriptional programs associated with increasingly hypoxic and metabolically stressed conditions secondary to overly dense cell cultures and lack of blood vessels to supply the increasingly thick tissue present in in vivo (Rankin et al., 2011). This could reflect a major limitation of this in vitro system when investigating late-stage differentiation.

Extracellular matrix makes up the major part of cartilage, providing the environment for differentiating chondrocytes. ECM composition is influenced by chondrocyte differentiation and health but vice versa, ECM may also influence chondrocyte differentiation and homeostasis via matrix-chondrocyte interactions (Gao et al., 2014). Hence, understanding the to date largely unresolved composition of ECM secreted by ATDC5 cells is of great interest. Here, we demonstrate that ATDC5 cells produce a more complex ECM than previously appreciated.

Of note, Wilhelm et al. applied a detailed fractionation protocol removing the majority of intracellular proteins but also risking losing some more loosely attached ECM components. In contrast, we only performed decellularization using a buffer composed of 20 mM NH_4OH and 0.5% Triton X-100, which likely preserved a broader spectrum of ECM proteins, but also intracellular components. To exclude these possibly retained intracellular proteins form our conclusions, we chose known ECM and matrisome proteins only to define ATDC5 components. Another factor that may have contributed to differences in the detected

ECM proteins is the use of slightly different differentiation media despite comparable culture durations. Wilhelm et al. supplemented the medium with insulin and from day 14 onward, DMEM/F12 was replaced with α-MEM medium and further supplemented with β-glycerophosphate. Our protocol included insulin, ascorbic acid, sodium selenite, and transferrin supplementation. Both protocols are established and may be used for ATDC5 differentiation, but differences in medium composition may influence matrix deposition and maturation and thereby affect the ECM proteins detected. Finally, differences in mass spectrometry platforms and data acquisition workflows, including the use of DIA-PASEF on a timsTOF fleX instrument in our study versus label-free LC-MALDI-based proteomics in Wilhelm et al., may also have contributed to differences in the proteins detected and to the higher number of proteins identified in our dataset.

Notably, the identified ECM proteins span all major functional categories, including structural components (collagens, proteoglycans), adaptor proteins (link proteins, matrilins, thrombospondins), surface receptors (integrins, CD44) and various ECM-modifying enzymes, indicating that ATDC5 cells may recapitulate multiple functional aspects of cartilage matrix biology. In our study, we additionally identified several collagens that were not previously reported, including minor collagens and fibril-associated Collagen IX, which co-localizes with Collagen II and X to stabilize the fibrillar network (Alcaide-Ruggiero et al., 2021). Matrilins (MATN1, MATN2, MATN4) were also detected, acting as adaptors between collagen fibrils and non-collagenous proteins (Wagener et al., 2005). Our protocol further allowed the identification of numerous secreted components, especially ECM remodeling enzymes, mineralization enzymes and secreted signalling proteins, suggesting ongoing matrix remodeling, calcification and extracellular signalling activity. Since our proteomic dataset presents a discovery-based resource, future studies using optimized ECM extraction protocols may provide additional validation of selected candidates.

Interestingly, neither we nor Willhelm et al. detected COMP, a key ECM protein with roles in promoting chondrogenesis and interacting with several ECM components (Posey et al., 2018), despite observations of increasing gene expression during differentiation in our study (Fig. 3 F). Other protein classes that were not well covered by our and Wilhelm et al.s̈ dataset comprised predominantly ECM enzymes involved in collagen catabolism and proteolysis. Several of them belong to the family of MMPs, ADAM (A Disintegrin and Metalloproteinase) or ADAMTS (A Disintegrin and Metalloproteinase with Thrombospondin motifs) proteins, which also have implications in osteoarthritis (Yang et al., 2017). While we detected some MMPs in our study (MMP11, MMP14, MMP19), we also missed a number, possibly due to low abundance.

Overall, consistent with the transcriptional increase of ECM and cartilage genes over time, ECM protein abundance also accumulated with ongoing differentiation, supporting the biological consistency of the model. In transcriptomic PCA, day 14 and day 21 samples clustered closely, indicating that the overall transcriptional state had not changed dramatically between these time points. In proteomics, however, day 21 samples appeared distinct from day 14, even though relatively few ECM proteins changed in abundance (Fig. 4 F), suggesting that intracellular proteins contribute to this separation. Consistent with transcriptomic analyses, the increased gene expression of *Aspn*, *Acan*, *Dcn*, *Fmod* and *Lum* at day 4 compared to day 0 corresponded with the detection of their proteins at day 4, which were not observed at earlier time points. Also, *Col10a1* gene expression increased markedly between day 7 and day 14 and was first detected at the protein level from day 14 onwards. The analysis of significantly and concordantly regulated ECM genes and proteins (Table 2) further confirmed that key ECM components are consistently increasing in expression during ATDC5 chondrogenic differentiation across both transcriptomic and proteomic datasets. These concordances underscore the consistency of our multi-omics approach. Taken together, these data indicate that under our experimental conditions, chondrogenic differentiation in ATDC5 cells is largely complete between day 14 and 21, consistent with the observed expression of Collagen X and decreased expression of major cartilage genes on day 21.

In summary, our time-resolved transcriptomic and ECM proteomic analysis demonstrates that ATDC5 cells capture key molecular and matrix-associated features of chondrogenic differentiation. However, limitations of the system, including the lack of typical zonal organization, disordered collagen fibril architecture, absence of mechanical loading, and confluence-related effects inherent to monolayer culture, should be considered when interpreting the data. Despite these limitations, the model captures major transcriptional programs and generates a complex cartilage-associated extracellular matrix, supporting its use as a well-characterized and accessible system for mechanistic studies of chondrogenesis and cartilage ECM biology.

CRediT authorship contribution statement

Anna Klawonn: Writing – original draft, Visualization, Investigation, Data curation. **Stefan Tholen:** Investigation, Data curation. **Ilona Skatulla:** Writing – review & editing, Project administration. **Chiara M. Schröder:** Visualization, Investigation, Data curation. **Sebastian J. Arnold:** Supervision, Resources, Funding acquisition. **Oliver Schilling:** Supervision, Resources, Funding acquisition. **Miriam Schmidts:** Writing – review & editing, Writing – original draft, Supervision, Resources, Project administration, Funding acquisition, Conceptualization.

Funding details

MS acknowledges funding from the Deutsche Forschungsgemeinschaft (DFG) Cilia FOR 5547 Cilia Dynamics (project 503306912) and SFB1597 SmallData (project 499552394). MS and SA acknowledge funding from the Deutsche Forschungsgemeinschaft (DFG), Cluster of Excellence, CIBBS – Centre for Integrative Biological Signalling Studies (EXC-2189, project 390939984) and MS and OS acknowledge funding from the Deutsche Forschungsgemeinschaft (DFG), SFB1543 NEPHGEN (project 431984000).

Declaration of competing interest

The authors declare that they have no known competing financial interests or personal relationships that could have appeared to influence the work reported in this paper.

Acknowledgement

We thank Christoph Schell and Maximilian Wess for helpful discussion of fibronectin immunofluorescence. The Proteomic Platform – Core Facility (ProtCF) was supported by the Medical Faculty of the University of Freiburg to Prof. Dr. Oliver Schilling (2021/A3-Sch and 2023/A3-Sch). We acknowledge the support of the Freiburg Galaxy Team, funded by the German Federal Ministry of Education and Research BMFTR grant 031 A538A de.NBI-RBC and the Ministry of Science, Research and the Arts Baden-Württemberg (MWK) within the framework of LIBIS/de.NBI Freiburg.

Appendix A. Supplementary data

Supplementary data to this article can be found online at https://doi.org/10.1016/j.bonr.2026.101924.

Data availability

RNA-seq data generated in this study have been deposited in the Gene Expression Omnibus (https://www.ncbi.nlm.nih.gov/geo/) under accession number GSE324360. Mass spectrometry raw data have been deposited at the ProteomeXchange Consortium (https://www.proteomexchange.org) under the accession number MSV000100830;

Reviewer account details: Username: "MSV000100830_reviewer", Password: "ST4796_Schmidts").

References

Akiyama, H., Chaboissier, M.C., Martin, J.F., Schedl, A., de Crombrugghe, B., 2002 Nov 1. The transcription factor Sox9 has essential roles in successive steps of the chondrocyte differentiation pathway and is required for expression of Sox5 and Sox6. Genes Dev. 16 (21), 2813–2828. https://doi.org/10.1101/gad.1017802. PubMed PMID: 12414734; PubMed Central PMCID: PMC187468.

Alcaide-Ruggiero, L., Molina-Hernández, V., Granados, M.M., Domínguez, J.M., 2021 Dec 11. Main and minor types of collagens in the articular cartilage: the role of collagens in repair tissue evaluation in chondral defects. Int. J. Mol. Sci. 22 (24), 13329. https://doi.org/10.3390/ijms222413329. PubMed PMID: 34948124; PubMed Central PMCID: PMC8706311.

Altaf, F.M., Hering, T.M., Kazmi, N.H., Yoo, J.U., Johnstone, B., Altaf, F.M., et al., 2006 Nov 9. Ascorbate-enhanced chondrogenesis of ATDC5 cells. Eur. Cells Mater. 12, 64–70. https://doi.org/10.22203/eCM.v012a08.

Atsumi, T., Miwa, Y., Kimata, K., Ikawa, Y., 1990 May. A chondrogenic cell line derived from a differentiating culture of AT805 teratocarcinoma cells. Cell Differ. Dev. 30 (2), 109–116. https://doi.org/10.1016/0922-3371(90)90079-c (PubMed PMID: 2201423).

Bačenková, D., Trebuňová, M., Demeterová, J., Živčák, J., 2023 Jan. Human chondrocytes, metabolism of articular cartilage, and strategies for application to tissue engineering. Int. J. Mol. Sci. 24 (23), 17096. https://doi.org/10.3390/ijms242317096.

Bartoletti, G., Dong, C., Umar, M., He, F., 2020 Oct 1. Pdgfra regulates multipotent cell differentiation towards chondrocytes via inhibiting Wnt9a/beta-catenin pathway during chondrocranial cartilage development. Dev. Biol. 466 (1–2), 36–46. https://doi.org/10.1016/j.ydbio.2020.08.004. PubMed PMID: 32800757; PubMed Central PMCID: PMC7494641.

Bubb, K., Holzer, T., Nolte, J.L., Krüger, M., Wilson, R., Schlötzer-Schrehardt, U., et al., 2021 Sep 22. Mitochondrial respiratory chain function promotes extracellular matrix integrity in cartilage. J. Biol. Chem. 297 (4), 101224. https://doi.org/10.1016/j.jbc.2021.101224. PubMed PMID: 34560099; PubMed Central PMCID: PMC8503590.

Busch, T., Neubauer, B., Schmitt, L., Cascante, I., Knoblich, L., Wegehaupt, O., et al., 2024. The role of the co-chaperone DNAJB11 in polycystic kidney disease: molecular mechanisms and cellular origin of cyst formation. FASEB J. 38 (21), e70162. https://doi.org/10.1096/fj.202401763R.

Caron, M.M.J., Eveque, M., Cillero-Pastor, B., Heeren, R.M.A., Housmans, B., Derks, K., et al., 2021 Jun 21. Sox9 determines translational capacity during early chondrogenic differentiation of ATDC5 cells by regulating expression of ribosome biogenesis factors and ribosomal proteins. Front. Cell Dev. Biol. 9, 686096. https://doi.org/10.3389/fcell.2021.686096. PubMed PMID: 34235151; PubMed Central PMCID: PMC8256280.

Casorati, B., Zafferri, I., Castiglioni, S., Maier, J.A., 2025 Apr. Replicative senescence in mesenchymal stem cells: an in vitro study on mitochondrial dynamics and metabolic alterations. Antioxidants 14 (4), 446. https://doi.org/10.3390/antiox14040446.

Česnik, A.B., Švajger, U., 2024 Jul 26. The issue of heterogeneity of MSC-based advanced therapy medicinal products–a review. Front. Cell Dev. Biol. 12. https://doi.org/10.3389/fcell.2024.1400347.

Challa, T.D., Rais, Y., Ornan, E.M., 2010 Jul 29. Effect of adiponectin on ATDC5 proliferation, differentiation and signaling pathways. Mol. Cell. Endocrinol. 323 (2), 282–291. https://doi.org/10.1016/j.mce.2010.03.025.

Chawla, S., Mainardi, A., Majumder, N., Dönges, L., Kumar, B., Occhetta, P., et al., 2022 Dec 13. Chondrocyte hypertrophy in osteoarthritis: mechanistic studies and models for the identification of new therapeutic strategies. Cells 11 (24), 4034. https://doi.org/10.3390/cells11244034. PubMed PMID: 36552796; PubMed Central PMCID: PMC9777397.

Chen, L., Fink, T., Zhang, X.Y., Ebbesen, P., Zachar, V., 2005 Sep 1. Quantitative transcriptional profiling of ATDC5 mouse progenitor cells during chondrogenesis. Differentiation 73 (7), 350–363. https://doi.org/10.1111/j.1432-0436.2005.00038.x.

Chen, L., Fink, T., Ebbesen, P., Zachar, V., 2006 Jun 10. Temporal transcriptome of mouse ATDC5 chondroprogenitors differentiating under hypoxic conditions. Exp. Cell Res. 312 (10), 1727–1744. https://doi.org/10.1016/j.yexcr.2006.02.013 (PubMed PMID: 16580664).

Cummins, E.P., Berra, E., Comerford, K.M., Ginouves, A., Fitzgerald, K.T., Seeballuck, F., et al., 2006 Nov 28. Prolyl hydroxylase-1 negatively regulates IkappaB kinase-beta, giving insight into hypoxia-induced NFkappaB activity. Proc. Natl. Acad. Sci. U. S. A. 103 (48), 18154–18159. https://doi.org/10.1073/pnas.0602235103. PubMed PMID: 17114296; PubMed Central PMCID: PMC1643842.

De la Fuente, A., Mateos, J., Lesende-Rodríguez, I., Calamia, V., Fuentes-Boquete, I., de Toro, F.J., et al., 2012 Feb 1. Proteome analysis during chondrocyte differentiation in a new chondrogenesis model using human umbilical cord stroma mesenchymal stem cells*. Mol. Cell. Proteomics 11 (2), M111.010496. https://doi.org/10.1074/mcp.M111.010496.

Demichev, V., Messner, C.B., Vernardis, S.I., Lilley, K.S., Ralser, M., 2020 Jan. DIA-NN: neural networks and interference correction enable deep proteome coverage in high throughput. Nat. Methods 17 (1), 41–44. https://doi.org/10.1038/s41592-019-0638-x.

Dong, X., Xu, X., Yang, C., Luo, Y., Wu, Y., Wang, J., 2021 Feb 1. USP7 regulates the proliferation and differentiation of ATDC5 cells through the Sox9-PTHrP-PTH1R axis. Bone 143, 115714. https://doi.org/10.1016/j.bone.2020.115714.

Engvall, E., Ruoslahti, E., 1977 Jul 15. Binding of soluble form of fibroblast surface protein, fibronectin, to collagen. Int. J. Cancer 20 (1), 1–5. https://doi.org/10.1002/ijc.2910200102 (PubMed PMID: 903179).

Farach-Carson, M.C., Wu, D., França, C.M., 2024. Proteoglycans in mechanobiology of tissues and organs: normal functions and mechanopathology. Proteoglycan Res. 2 (2), e21. https://doi.org/10.1002/pgr2.21. PubMed PMID: 39584146; PubMed Central PMCID: PMC11584024.

Farcasanu, M.V., Ruiz, T. de las H., Brito, F.M.J. de S., Soul, J., Coxhead, J., German, M. J., et al., 2025. Dynamic compression improves chondrogenesis in the tissue engineered model of cartilage. Biotechnol. Bioeng. 122 (9), 2574–2591. https://doi.org/10.1002/bit.29026.

Gao, Y., Liu, S., Huang, J., Guo, W., Chen, J., Zhang, L., et al., 2014. The ECM-cell interaction of cartilage extracellular matrix on chondrocytes. Biomed. Res. Int. 2014, 648459. https://doi.org/10.1155/2014/648459. PubMed PMID: 24959581; PubMed Central PMCID: PMC4052144.

Georgieva, V.S., Etich, J., Bluhm, B., Zhu, M., Frie, C., Wilson, R., et al., 2020 Jan. Ablation of the miRNA cluster 24 has profound effects on extracellular matrix protein abundance in cartilage. Int. J. Mol. Sci. 21 (11), 4112. https://doi.org/10.3390/ijms21114112.

Goldring, M.B., Tsuchimochi, K., Ijiri, K., 2006 Jan 1. The control of chondrogenesis. J. Cell. Biochem. 97 (1), 33–44. https://doi.org/10.1002/jcb.20652 (PubMed PMID: 16215986).

Gottardi, R., Hansen, U., Raiteri, R., Loparic, M., Düggelin, M., Mathys, D., et al., 2016 Oct 25. Supramolecular organization of collagen fibrils in healthy and osteoarthritic human knee and hip joint cartilage. PloS One 11 (10), e0163552. https://doi.org/10.1371/journal.pone.0163552.

Grässel, S., Aszódi, A. (Eds.), 2016. Cartilage [Internet]. Springer International Publishing, Cham. https://doi.org/10.1007/978-3-319-29568-8 [cited 2026 Jan 24]. Available from: http://link.springer.com/10.1007/978-3-319-29568-8.

Gu, J., Lu, Y., Li, F., Qiao, L., Wang, Q., Li, N., et al., 2014 Oct. Identification and characterization of the novel Col10a1 regulatory mechanism during chondrocyte hypertrophic differentiation. Cell Death Dis. 5 (10), e1469. https://doi.org/10.1038/cddis.2014.444. PubMed PMID: 25321476; PubMed Central PMCID: PMC4649528.

Han, L., Grodzinsky, A.J., Ortiz, C., 2011 Jul 1. Nanomechanics of the cartilage extracellular matrix. Annu. Rev. Mater. Res. 41, 133–168. https://doi.org/10.1146/annurev-matsci-062910-100431. PubMed PMID: 22792042; PubMed Central PMCID: PMC3392687.

Heberle, H., Meirelles, G.V., da Silva, F.R., Telles, G.P., Minghim, R., 2015 May 22. InteractiVenn: a web-based tool for the analysis of sets through Venn diagrams. BMC Bioinformatics 16 (1), 169. https://doi.org/10.1186/s12859-015-0611-3.

Hissnauer, T.N., Baranowsky, A., Pestka, J.M., Streichert, T., Wiegandt, K., Goepfert, C., et al., 2010 Dec 1. Identification of molecular markers for articular cartilage. Osteoarthr. Cartil. 18 (12), 1630–1638. https://doi.org/10.1016/j.joca.2010.10.002.

Hodax, J.K., Quintos, J.B., Gruppuso, P.A., Chen, Q., Desai, S., Jayasuriya, C.T., 2019 Jun 17. Aggrecan is required for chondrocyte differentiation in ATDC5 chondroprogenitor cells. PloS One 14 (6), e0218399. https://doi.org/10.1371/journal.pone.0218399.

Hodgkinson, C.P., Naidoo, V., Patti, K.G., Gomez, J.A., Schmeckpeper, J., Zhang, Z., et al., 2013 Aug. Abi3bp is a multifunctional autocrine/paracrine factor that regulates mesenchymal stem cell biology. Stem Cells Dayt Ohio 31 (8), 1669–1682. https://doi.org/10.1002/stem.1416. PubMed PMID: 23666637; PubMed Central PMCID: PMC3775980.

Holm, E., Gleberzon, J.S., Liao, Y., Sørensen, E.S., Beier, F., Hunter, G.K., et al., 2014 Dec 5. Osteopontin mediates mineralization and not osteogenic cell development in vitro. Biochem. J. 464 (3), 355–364. https://doi.org/10.1042/BJ20140702.

Horkay, F., Basser, P.J., Hecht, A.M., Geissler, E., 2017. Structure and properties of cartilage proteoglycans. Macromol. Symp. 372 (1), 43–50. https://doi.org/10.1002/masy.201700014.

Hsueh, M.F., Khabut, A., Kjellström, S., Önnerfjord, P., Kraus, V.B., 2016 Feb 5. Elucidating the molecular composition of cartilage by proteomics. J. Proteome Res. 15 (2), 374–388. https://doi.org/10.1021/acs.jproteome.5b00946. PubMed PMID: 26632656; PubMed Central PMCID: PMC4917199.

Huitema, L.F.A., Vaandrager, A.B., van Weeren, P.R., Barneveld, A., Helms, J.B., van de Lest, C.H.A., 2006 Mar. The nitric oxide donor sodium nitroprusside inhibits mineralization in ATDC5 cells. Calcif. Tissue Int. 78 (3), 171–177. https://doi.org/10.1007/s00223-005-1233-y (PubMed PMID: 16523220).

Huynh, N.P.T., Zhang, B., Guilak, F., 2019 Jan. High-depth transcriptomic profiling reveals the temporal gene signature of human mesenchymal stem cells during chondrogenesis. FASEB J. 33 (1), 358–372. https://doi.org/10.1096/fj.201800534R. PubMed PMID: 29985644; PubMed Central PMCID: PMC6355072.

Jia, Y., Le, H., Wang, X., Zhang, J., Liu, Y., Ding, J., et al., 2023 Nov 20. Double-edged role of mechanical stimuli and underlying mechanisms in cartilage tissue engineering. Front. Bioeng. Biotechnol. 11. https://doi.org/10.3389/fbioe.2023.1271762.

Kiani, C., Chen, L., Wu, Y.J., Yee, A.J., Yang, B.B., 2002 Mar. Structure and function of aggrecan. Cell Res. 12 (1), 19–32. https://doi.org/10.1038/sj.cr.7290106.

Kim, I.S., Otto, F., Zabel, B., Mundlos, S., 1999 Feb. Regulation of chondrocyte differentiation by Cbfa1. Mech. Dev. 80 (2), 159–170. https://doi.org/10.1016/s0925-4773(98)00210-x (PubMed PMID: 10072783).

Kim, D.S., Lee, M.W., Lee, T.H., Sung, K.W., Koo, H.H., Yoo, K.H., 2017 Mar. Cell culture density affects the stemness gene expression of adipose tissue-derived mesenchymal stem cells. Biomed. Rep. 6 (3), 300–306. https://doi.org/10.3892/br.2017.845. PubMed PMID: 28451390; PubMed Central PMCID: PMC5403436.

Lawrence, J.E.G., Woods, S., Roberts, K., Sumanaweera, D., Balogh, P., Li, T., et al., 2025 Nov 17. Single-cell transcriptomics identifies chondrocyte differentiation dynamics in vivo and in vitro. Dev. Cell 60 (22), 3066–3084.e8. https://doi.org/10.1016/j.devcel.2025.06.031.

LeBlanc, L., Kim, M., Kambhampati, A., Son, A.J., Ramirez, N., Kim, J., 2022 Jan 21. β-catenin links cell seeding density to global gene expression during mouse embryonic stem cell differentiation. iScience 25 (1). https://doi.org/10.1016/j.isci.2021.103541 (PubMed PMID: 34977504).

Lefebvre, V., Dvir-Ginzberg, M., 2017 Jan. SOX9 and the many facets of its regulation in the chondrocyte lineage. Connect. Tissue Res. 58 (1), 2–14. https://doi.org/10.1080/03008207.2016.1183667. PubMed PMID: 27128146; PubMed Central PMCID: PMC5287363.

Leung, V.Y.L., Gao, B., Leung, K.K.H., Melhado, I.G., Wynn, S.L., Au, T.Y.K., et al., 2011 Nov 3. SOX9 governs differentiation stage-specific gene expression in growth plate chondrocytes via direct concomitant transactivation and repression. PLoS Genet. 7 (11), e1002356. https://doi.org/10.1371/journal.pgen.1002356.

Liang, T., Li, P., Liang, A., Zhu, Y., Qiu, X., Qiu, J., et al., 2022 Nov 15. Identifying the key genes regulating mesenchymal stem cells chondrogenic differentiation: an in vitro study. BMC Musculoskelet. Disord. 23 (1), 985. https://doi.org/10.1186/s12891-022-05958-7.

Luo, Z., Tian, M., Yang, G., Tan, Q., Chen, Y., Li, G., et al., 2022 Jul 7. Hypoxia signaling in human health and diseases: implications and prospects for therapeutics. Signal Transduct. Target. Ther. 7 (1), 218. https://doi.org/10.1038/s41392-022-01080-1.

Makhijani, P., Basso, P.J., Chan, Y.T., Chen, N., Baechle, J., Khan, S., et al., 2023 Mar 13. Regulation of the immune system by the insulin receptor in health and disease. Front. Endocrinol. 14, 1128622. https://doi.org/10.3389/fendo.2023.1128622. PubMed PMID: 36992811; PubMed Central PMCID: PMC10040865.

Moger, C.J., Barrett, R., Bleuet, P., Bradley, D.A., Ellis, R.E., Green, E.M., et al., 2007 Jun 1. Regional variations of collagen orientation in normal and diseased articular cartilage and subchondral bone determined using small angle X-ray scattering (SAXS). Osteoarthr. Cartil. 15 (6), 682–687. https://doi.org/10.1016/j.joca.2006.12.006.

Molin, A.N., Contentin, R., Angelozzi, M., Karvande, A., Kc, R., Haseeb, A., et al., 2024 Feb 20. Skeletal growth is enhanced by a shared role for SOX8 and SOX9 in promoting reserve chondrocyte commitment to columnar proliferation. Proc. Natl. Acad. Sci. 121 (8), e2316969121. https://doi.org/10.1073/pnas.2316969121.

Neame, P.J., Barry, F.P., 1993 May 1. The link proteins. Experientia 49 (5), 393–402. https://doi.org/10.1007/BF01923584.

Newton, P.T., Staines, K.A., Spevak, L., Boskey, A.L., Teixeira, C.C., Macrae, V.E., et al., 2012 Nov. Chondrogenic ATDC5 cells: an optimised model for rapid and physiological matrix mineralisation. Int. J. Mol. Med. 30 (5), 1187–1193. https://doi.org/10.3892/ijmm.2012.1114 (PubMed PMID: 22941229; PubMed Central PMCID: PMC3573767).

Okita, K., Hikiji, H., Koga, A., Nagai-Yoshioka, Y., Yamasaki, R., Mitsugi, S., et al., 2023. Ascorbic acid enhances chondrocyte differentiation of ATDC5 by accelerating insulin receptor signaling. Cell Biol. Int. 47 (10), 1737–1748. https://doi.org/10.1002/cbin.12067.

Paten, J.A., Martin, C.L., Wanis, J.T., Siadat, S.M., Figueroa-Navedo, A.M., Ruberti, J.W., et al., 2019 Aug 8. Molecular interactions between collagen and fibronectin: a reciprocal relationship that regulates *de novo* fibrillogenesis. Chem 5 (8), 2126–2145. https://doi.org/10.1016/j.chempr.2019.05.011.

Posey, K.L., Coustry, F., Hecht, J.T., 2018 Oct. Cartilage oligomeric matrix protein: COMPopathies and beyond. Matrix Biol. 71–72, 161–173. https://doi.org/10.1016/j.matbio.2018.02.023. PubMed PMID: 29530484; PubMed Central PMCID: PMC6129439.

Rankin, E.B., Giaccia, A.J., Schipani, E., 2011 Jun. A central role for hypoxic signaling in cartilage, bone, and hematopoiesis. Curr. Osteoporos. Rep. 9 (2), 46–52. https://doi.org/10.1007/s11914-011-0047-2. PubMed PMID: 21360287; PubMed Central PMCID: PMC4012534.

Riss, T.L., Moravec, R.A., Duellman, S.J., Niles, A.L., 2021 Dec 1. Treating cells as reagents to design reproducible assays. SLAS Discov. 26 (10), 1256–1267. https://doi.org/10.1177/24725552211039754. Special Issue: Assay Guidance Manual for Drug Discovery: Robust or Go Bust.

Ritchie, M.E., Phipson, B., Wu, D., Hu, Y., Law, C.W., Shi, W., et al., 2015 Apr 20. Limma powers differential expression analyses for RNA-sequencing and microarray studies. Nucleic Acids Res. 43 (7), e47. https://doi.org/10.1093/nar/gkv007.

Schwarzl, T., Keogh, A., Shaw, G., Krstic, A., Clayton, E., Higgins, D.G., et al., 2023 Nov 3. Transcriptional profiling of early differentiation of primary human mesenchymal stem cells into chondrocytes. Sci. Data 10 (1), 758. https://doi.org/10.1038/s41597-023-02686-y.

Sebastian, A., JL, McCool, Hum, N.R., Murugesh, D.K., Wilson, S.P., Christiansen, B.A., et al., 2021 Jun. Single-cell RNA-Seq reveals transcriptomic heterogeneity and post-traumatic osteoarthritis-associated early molecular changes in mouse articular chondrocytes. Cells 10 (6), 1462. https://doi.org/10.3390/cells10061462.

Shao, X., Gomez, C.D., Kapoor, N., Considine, J.M., Grams, C., Gao, Y. (Tom), et al., 2023 Jan 6. MatrisomeDB 2.0: 2023 updates to the ECM-protein knowledge database. Nucleic Acids Res. 51 (D1), D1519–D1530. https://doi.org/10.1093/nar/gkac1009.

Shea, C.M., Edgar, C.M., Einhorn, T.A., Gerstenfeld, L.C., 2003. BMP treatment of C3H10T1/2 mesenchymal stem cells induces both chondrogenesis and osteogenesis. J. Cell. Biochem. 90 (6), 1112–1127. https://doi.org/10.1002/jcb.10734.

Sherman, B.T., Hao, M., Qiu, J., Jiao, X., Baseler, M.W., Lane, H.C., et al., 2022 Jul 5. DAVID: a web server for functional enrichment analysis and functional annotation of gene lists (2021 update). Nucleic Acids Res. 50 (W1), W216–W221. https://doi.org/10.1093/nar/gkac194. PubMed PMID: 35325185; PubMed Central PMCID: PMC9252805.

Shukunami, C., Ishizeki, K., Atsumi, T., Ohta, Y., Suzuki, F., Hiraki, Y., 1997. Cellular hypertrophy and calcification of embryonal carcinoma-derived chondrogenic cell line ATDC5 in vitro. J. Bone Miner. Res. 12 (8), 1174–1188. https://doi.org/10.1359/jbmr.1997.12.8.1174.

Shukunami, C., Ohta, Y., Sakuda, M., Hiraki, Y., 1998 May 25. Sequential progression of the differentiation program by bone morphogenetic protein-2 in chondrogenic cell line ATDC5. Exp. Cell Res. 241 (1), 1–11. https://doi.org/10.1006/excr.1998.4045 (PubMed PMID: 9633508).

Sive, J.I., Baird, P., Jeziorsk, M., Watkins, A., Hoyland, J.A., Freemont, A.J., 2002 Apr. Expression of chondrocyte markers by cells of normal and degenerate intervertebral discs. Mol. Pathol. 55 (2), 91–97. https://doi.org/10.1136/mp.55.2.91. PubMed PMID: 11950957; PubMed Central PMCID: PMC1187156.

Surmann-Schmitt, C., Dietz, U., Kireva, T., Adam, N., Park, J., Tagariello, A., et al., 2008 Mar 14. Ucma, a novel secreted cartilage-specific protein with implications in osteogenesis. J. Biol. Chem. 283 (11), 7082–7093. https://doi.org/10.1074/jbc.M702792200 (PubMed PMID: 18156182).

Svensson, R.B., Hassenkam, T., Grant, C.A., Magnusson, S.P., 2010 Dec 15. Tensile properties of human collagen fibrils and fascicles are insensitive to environmental salts. Biophys. J. 99 (12), 4020–4027. https://doi.org/10.1016/j.bpj.2010.11.018. PubMed PMID: 21156145; PubMed Central PMCID: PMC3000511.

Tare, R.S., Howard, D., Pound, J.C., Roach, H.I., Oreffo, R.O.C., 2005 Jul 29. Tissue engineering strategies for cartilage generation—micromass and three dimensional cultures using human chondrocytes and a continuous cell line. Biochem. Biophys. Res. Commun. 333 (2), 609–621. https://doi.org/10.1016/j.bbrc.2005.05.117.

Tchetina, E., Mwale, F., Poole, A., 2003. Distinct phases of coordinated early and late gene expression in growth plate chondrocytes in relationship to cell proliferation, matrix assembly, remodeling, and cell differentiation. J. Bone Miner. Res. 18 (5), 844–851. https://doi.org/10.1359/jbmr.2003.18.5.844.

Temu, T.M., Wu, K.Y., Gruppuso, P.A., Phornphutkul, C., 2010 Aug. The mechanism of ascorbic acid-induced differentiation of ATDC5 chondrogenic cells. Am. J. Physiol. Endocrinol. Metab. 299 (2), E325–E334. https://doi.org/10.1152/ajpendo.00145.2010. PubMed PMID: 20530736; PubMed Central PMCID: PMC2928517.

Unger, S., Ferreira, C.R., Mortier, G.R., Ali, H., Bertola, D.R., Calder, A., et al., 2023 May. Nosology of genetic skeletal disorders: 2023 revision. Am. J. Med. Genet. A 191 (5), 1164–1209. https://doi.org/10.1002/ajmg.a.63132 PubMed PMID: 36779427; PubMed Central PMCID: PMC10081954.

Vidak, E., Javoršek, U., Vizovišek, M., Turk, B., 2019 Mar 20. Cysteine cathepsins and their extracellular roles: shaping the microenvironment. Cells 8 (3), 264. https://doi.org/10.3390/cells8030264. PubMed PMID: 30897858; PubMed Central PMCID: PMC6468544.

Wagener, R., Ehlen, H.W.A., Ko, Y.P., Kobbe, B., Mann, H.H., Sengle, G., et al., 2005 Jun 13. The Matrilins – adaptor proteins in the extracellular matrix. FEBS Lett. 579 (15), 3323–3329. https://doi.org/10.1016/j.febslet.2005.03.018. Budapest Special Issue.

Wang, Y., Middleton, F., Horton, J.A., Reichel, L., Farnum, C.E., Damron, T.A., 2004 Dec 1. Microarray analysis of proliferative and hypertrophic growth plate zones identifies differentiation markers and signal pathways. Bone 35 (6), 1273–1293. https://doi.org/10.1016/j.bone.2004.09.009.

Welsh, B.L., Sikder, P., 2025. Advancements in cartilage tissue engineering: a focused review. J. Biomed. Mater. Res. B Appl. Biomater. 113 (1), e35520. https://doi.org/10.1002/jbm.b.35520.

Wilhelm, D., Kempf, H., Bianchi, A., Vincourt, J.B., 2020 May 15. ATDC5 cells as a model of cartilage extracellular matrix neosynthesis, maturation and assembly. J. Proteomics 219, 103718. https://doi.org/10.1016/j.jprot.2020.103718.

Wu, C.L., Dicks, A., Steward, N., Tang, R., Katz, D.B., Choi, Y.R., et al., 2021 Jan 13. Single cell transcriptomic analysis of human pluripotent stem cell chondrogenesis. Nat. Commun. 12, 362. https://doi.org/10.1038/s41467-020-20598-y. PubMed PMID: 33441552; PubMed Central PMCID: PMC7806634.

Yang, C.Y., Chanalaris, A., Troeberg, L., 2017 Jul. ADAMTS and ADAM metalloproteinases in osteoarthritis – looking beyond the 'usual suspects.'. Osteoarthritis Cartilage 25 (7), 1000–1009. https://doi.org/10.1016/j.joca.2017.02.791. PubMed PMID: 28216310; PubMed Central PMCID: PMC5473942.

Yuan, Z., Liu, S., Song, W., Liu, Y., Bi, G., Xie, R., et al., 2022 May 9. Galactose enhances chondrogenic differentiation of ATDC5 and cartilage matrix formation by chondrocytes. Front. Mol. Biosci. 9. https://doi.org/10.3389/fmolb.2022.850778.

Zhao, Q., Eberspaecher, H., Lefebvre, V., De Crombrugghe, B., 1997 Aug. Parallel expression of Sox9 and Col2a1 in cells undergoing chondrogenesis. Dev Dyn Off Publ Am Assoc Anat. 209 (4), 377–386. https://doi.org/10.1002/(SICI)1097-0177(199708)209:4<377::AID-AJA5>3.0.CO;2-F (PubMed PMID: 9264261).

Zhou, J., Li, C., Yu, A., Jie, S., Du, X., Liu, T., et al., 2019 Jul. Bioinformatics analysis of differentially expressed genes involved in human developmental chondrogenesis. Medicine (Baltimore) 98 (27), e16240. https://doi.org/10.1097/MD.0000000000016240.

Ziros, P.G., Basdra, E.K., Papavassiliou, A.G., 2008. Runx2: of bone and stretch. Int. J. Biochem. Cell Biol. 40 (9), 1659–1663. https://doi.org/10.1016/j.biocel.2007.05.024 (PubMed PMID: 17656144).